Surface-mediated Bacteriophage Defense Incurs Fitness Tradeoffs for Interbacterial Antagonism

Chia-En Tsai[1,2,5], Feng-Qi Wang[2,5], Chih-Wen Yang[3], Ling-Li Yang[2], Thao V. Nguyen[2], Yung-Chih Chen[2], Po-Yin Chen[1,2], Ing-Shouh Hwang[3], See-Yeun Ting[1,2,4†]

[1] Molecular and Cell Biology, Taiwan International Graduate Program, Academia Sinica and National Defense Medical Center, Taipei, 11490, Taiwan

[2] Institute of Molecular Biology, Academia Sinica, Taipei 11529, Taiwan

[3] Institute of Physics, Academia Sinica, Taipei 115201, Taiwan

[4] Genome and Systems Biology Degree Program, National Taiwan University, Taipei 106319, Taiwan

[5] These authors contributed equally

[†]Correspondence: syting@gate.sinica.edu.tw

Keywords:

Phage; Lipopolysaccharide; Interbacterial Antagonism; Bacterial Immunity; Tail Spike Protein

ABSTRACT

Bacteria in polymicrobial habitats are constantly exposed to biotic threats from bacteriophages (or "phages"), antagonistic bacteria, and predatory eukaryotes. These antagonistic interactions play crucial roles in shaping the evolution and physiology of bacteria. To survive, bacteria have evolved mechanisms to protect themselves from such attacks, but the fitness costs of resisting one threat and rendering bacteria susceptible to others remain unappreciated. Here, we examined the fitness consequences of phage resistance in *Salmonella enterica*, revealing that phage-resistant variants exhibited significant fitness loss upon co-culture with competitor bacteria. These phage-resistant strains display varying degrees of lipopolysaccharide (LPS) deficiency and increased susceptibility to contact-dependent interbacterial antagonism, such as the type VI secretion system (T6SS). Utilizing mutational analyses and atomic force microscopy, we show that the long-modal length O-antigen of LPS serves as a protective barrier against T6SS-mediated intoxication. Notably, this competitive disadvantage can also be triggered independently by phages possessing LPS-targeting endoglycosidase in their tail spike proteins, which actively cleave the O-antigen upon infection. Our findings reveal two distinct mechanisms of phage-mediated LPS modifications that modulate interbacterial competition, shedding light on the dynamic microbial interplay within mixed populations.

38 **INTRODUCTION**

39 Microbial communities are frequently subjected to antagonistic interactions within their
40 environments, predominantly from phages, bacterial competitors, and unicellular predatory
41 eukaryotes. Phages, the most abundant biological entities on Earth, possess the capacity to
42 devastate entire bacterial populations through lytic cycles[1]. Similarly, bacterial competitors
43 employ a diverse array of specialized mechanisms, such as the production of antibiotics, secretion
44 of antimicrobial peptides, deployment of toxin delivery systems, and utilization of membrane-
45 puncturing nanomachines, all aimed at inhibiting or killing rival bacteria[2-5]. Moreover, unicellular
46 eukaryotic predators, such as free-living protozoa, exert predation pressure on bacterial
47 populations through phagocytosis[6]. Collectively, these antagonistic interactions impose significant
48 selective pressures on bacteria that profoundly influence their evolution, ecology, and physiology.

49 To survive in such hostile environments, bacteria have evolved a broad spectrum of defense
50 mechanisms against biotic threats[7]. To mitigate or evade phage infection, bacteria have developed
51 strategies targeting nearly every stage of the phage life cycle[8]. Extracellular defenses, including
52 mutations or downregulation of surface receptors (*e.g.,* membrane proteins and
53 lipopolysaccharides), can prevent phage attachment and subsequent infection[9, 10]. Intracellularly,
54 widely distributed defense systems—such as restriction-modification systems, CRISPR-Cas
55 systems, and abortive infection mechanisms, act to neutralize phages post-entry[8, 11, 12]. Parallel to
56 these antiviral defenses, bacteria have also evolved strategies to counteract the antagonism posed
57 by competitor bacteria. For instance, the acquisition of immunity determinants endows resistance
58 against specific interbacterial toxins and antimicrobial compounds[13, 14]. Furthermore, general
59 stress responses and competition-sensing pathways enhance bacterial resilience to antimicrobial
60 agents in both environmental and clinical contexts[15-17]. This dynamic interplay between microbial

61 offense and defense underscores the central importance of these interactions in shaping microbial
62 communities.

63 Although biotic pressures imposed by other microbes significantly drive the evolution of
64 bacterial immunity, accumulating evidence indicates that this evolutionary process is frequently
65 associated with fitness trade-offs[18]. A prominent example is bacterial surface modifications that
66 hinder phage attachment but concurrently compromise bacterial fitness upon encountering
67 antibiotics or host immune systems[10, 19-21]. Similarly, CRISPR-Cas immunity has been shown to
68 impose an increased metabolic burden on host cells, which may limit its distribution across
69 bacterial taxa[22-25]. Furthermore, though a mucoid phenotype confers partial protection against
70 phage infection, it often incurs fitness costs in the context of bacterial competition[26-28]. Recent
71 research on *Escherichia coli* has also demonstrated that genetic variants resistant to interbacterial
72 intoxication may suffer from growth defects and increased susceptibility to antimicrobial agents
73 and environmental stresses[29]. Such fitness trade-offs associated with antagonistic coevolution are
74 highly context-dependent[30], but predicting their impact on microbial community composition
75 remains challenging due to the mechanisms underlying these fitness costs frequently being poorly
76 characterized.

77 In this study, we report that though bacteria develop surface modifications to protect
78 against viral infection, these modifications result in significant trade-offs in interbacterial
79 competition with antagonistic bacteria. We provide evidence that lipopolysaccharide (LPS), a
80 major component of the bacterial outer membrane, plays a previously unappreciated role in
81 protecting against contact-dependent killing by bacterial competitors. Remarkably, we have
82 discovered that mutations in LPS biosynthesis genes, as well as interactions with phages encoding
83 LPS-targeting endoglycosidase in their tail spike proteins, contribute to the observed competitive

disadvantage. Our study identifies two distinct mechanisms by which phage-mediated LPS modifications influence interbacterial competition, highlighting the role of antagonistic coevolution in shaping bacterial composition within polymicrobial communities.

RESULTS

Phage-resistant *S. enterica* Displays Competitive Fitness Deficits in Co-culture with Bacterial Competitors

To investigate if phage-resistant bacteria incur fitness consequences when interacting with bacterial competitors, we began by obtaining phage-resistant variants of the model bacterium, *Salmonella enterica* serovar Typhimurium, from an established transposon insertion library for pairwise bacterial co-culture experiments[31, 32] (**Figure 1a**). We reasoned that using this model bacterium and the mutant library would facilitate the identification of underlying pathways associated with competitive fitness costs. Consequently, we isolated distinct *S. enterica* variants that were resistant to model phages from different families of Caudovirales: Felix O1 (Myoviridae)[33], P22 (Podoviridae)[34], and Chi (Siphoviridae)[35] (**Supplementary Figure 1a, b**). Mutants exhibiting no significant growth defects under standard conditions were selected for further analysis (**Supplementary Figures 1c, d**). We then co-cultured individual strains with competitor bacteria, *i.e.*, Enterohemorrhagic *Escherichia coli* (EHEC) or *Enterobacter cloacae,* in a one-to-one ratio in both liquid and solid media. We selected EHEC and *E. cloacae* due to their ecological overlap with *S. enterica* in the mammalian gastrointestinal tract, where they frequently co-occur during infections, representing a relevant model for studying competitive interactions in both environmental and clinical contexts[36-38].

106 Compared to the wild-type *S. enterica* strain, we found that none of the phage-resistant
107 mutants exhibited competitive fitness differences in liquid broth co-culture assays with EHEC or
108 *E. cloacae* (**Figure 1b**). However, in solid media, though phage-resistant mutants exhibited no
109 observable fitness cost when incubated with EHEC, strains resistant to the Felix O1 and P22
110 phages displayed significant competitive disadvantage (relative survival < 1) upon co-culture with
111 *E. cloacae* (**Figure 1c**). This competitive phenotype was restricted to solid media, where cell-cell
112 contacts are relatively stable, indicating that the stress imposed by *E. cloacae* is likely contact-
113 dependent[39]. Interestingly, resistant strains against phage Chi did not present a similar fitness
114 disadvantage, indicating that phage-specific resistance mechanisms might underlie the competitive
115 trade-offs in *S. enterica* (**Figure 1c**). These findings prompted us to prioritize investigating: (1)
116 which gene mutations in *S. enterica* conferring resistance to phages Felix O1 and P22 impose
117 interbacterial competitive disadvantages on the bacteria; and (2) what mechanism in *E. cloacae* is
118 critical for the competitive phenotype observed in our co-culture assay.
119

120 **Mutations in LPS Biosynthesis Genes Confer Competitive Disadvantages on *S. enterica***

121 To escape viral infection, bacteria often evolve and modify their surface receptors to
122 prevent phage entry[40]. Previous studies have identified LPS on the outer bacterial membrane as
123 the primary receptor for phages Felix O1 and P22[41, 42]. Accordingly, we postulated that our phage-
124 resistant *S. enterica* strains likely harbor mutations in LPS-related genes, thereby influencing their
125 susceptibility to *E. cloacae*. Indeed, we identified disruptive transposon insertions concentrated in
126 genes associated with the LPS biosynthesis pathway in our phage-resistant strains, indicating an
127 impairment in the outer membrane cell envelope of these mutants (**Supplementary Figures 2a,**
128 **b**). To confirm this finding, we compared LPS levels in these mutants relative to the wild-type

129 strain. LPS PAGE profiles revealed a significant reduction in LPS levels, particularly of the O-
130 antigen, in the Felix O1- and P22-resistant strains compared to wild-type (**Figures 2a, b**). In
131 contrast, the phage Chi-resistant *S. enterica* variants had transposon insertions in genes unrelated
132 to LPS biosynthesis, and their LPS levels were comparable to wild-type bacteria (Supplementary
133 **Figures 2c, d**). Additionally, many of the Felix O1- and P22-resistant strains exhibited auto-
134 aggregation in unicellular culture (**Supplementary Figures 2e, f**), a phenotype associated with
135 LPS deficiency[43, 44]. These findings indicate that disruption of LPS biosynthesis genes contributes
136 to the competitive fitness defects observed in *S. enterica* co-cultured with *E. cloacae* (**Figure 1c**).
137

138 **Phage-resistant *S. enterica* Strains are More Susceptible to T6SS-mediated Intoxication**

139 Next, we sought to elucidate the underlying cell contact-dependent mechanisms utilized by
140 *E. cloacae* in competing with *S. enterica*. Prior studies have shown that *E. cloacae* relies on
141 functional secretory systems, such as the type VI secretion system (T6SS) and the contact-
142 dependent growth inhibition (CDI) pathway, to outcompete their bacterial rivals[45, 46]. These
143 secretory systems translocate antibacterial toxins into neighboring cells upon direct cell-cell
144 interaction, facilitating potent mechanisms of contact-dependent intoxication between bacteria[47,
145 48]. Therefore, we hypothesized that the competitive fitness trade-offs observed in the phage-
146 resistant strains might be attributable to interbacterial antagonism mediated by these secretory
147 systems.

148 To determine if such antagonistic pathways in *E. cloacae* contribute to the competitive
149 defects of the Felix O1- and P22-resistant *S. enterica* strains, we subjected them to pairwise
150 competition under contact-promoting conditions against *E. cloacae* mutant strains in which the
151 T6SS (Δ*tssM*) or CDI (Δ*cdiA*) had been inactivated[45, 46]. Consistent with our co-culture

152 experiments, the phage-resistant variants displayed reduced competitiveness when incubated with
153 wild-type *E. cloacae* (**Figures 2c, d**). Notably, T6SS inactivation abrogated the competitive defect
154 of the phage-resistant strains, whereas the competitive phenotype persisted in competition with *E.*
155 *cloacae* Δ*cdiA* (**Figures 2e-h**). These results support the notion that the competitive fitness deficit
156 in the phage-resistant strains arises from T6SS-mediated interbacterial antagonism.
157

158 **LPS O-antigen Protects *S. enterica* from T6SS-mediated Assaults**

159 Although the T6SS is an effective antibacterial mechanism, target cells can evade being
160 killed by avoiding direct contact with bacteria possessing an active T6SS[49]. One strategy to do so
161 is for target cells to produce extracellular biopolymers, such as secreted exopolysaccharides,
162 membrane-attached capsules, or colanic acid, all of which may act as a physical barrier against
163 T6SS-mediated attacks[15, 50, 51]. LPS, a major component of Gram-negative bacterial surfaces, is
164 known to confer protection against external stresses such as antibiotics, antimicrobial peptides,
165 and host immune systems[52, 53]. Therefore, the observed competitive disadvantage we observed in
166 LPS-deficient *S. enterica* led us to explore the function of LPS in protecting against T6SS-
167 mediated assaults.

168 LPS is comprised of lipid A covalently linked to core oligosaccharides (core OS) and
169 repetitive O-units (O-antigen) (**Figure 3a**). First, we sought to determine if the sugar composition
170 of the core OS is involved in protecting *S. enterica* against T6SS. We constructed in-frame
171 deletions of LPS-related genes in *S. enterica* differing in core OS structures (*i.e.,* WaaL, WaaJ,
172 WaaO, WaaG for the main chain OS structure, or WaaK, WaaB, WaaQ, WaaY for the side chain)[54]
173 (**Figure 3a**). If the LPS structure exerts a protective role, we anticipated that mutants hosting these
174 mutated genes would exhibit competitive fitness defects upon co-incubation with *E. cloacae*

175 carrying an active T6SS. Indeed, though mutations in the LPS-related genes did not result in
176 significant growth defects in unicellular cultures (**Supplementary Figures 3a-c**), strains deficient
177 in the genes essential for building the main chain OS structure displayed lower interbacterial
178 competitiveness than the wild-type strain (**Figures 3b, c** and **Supplementary Figure 3d**), similar
179 to the results we observed for LPS-deficient phage-resistant variants (**Figures 2c, d**). In contrast,
180 *S. enterica* mutants in which the side chain OS structure was perturbed presented indistinguishable
181 competitiveness to wild-type, except for the WaaK-deficient strain (**Figures 3d, e** and
182 **Supplementary Figure 3e**). Previous studies demonstrated that WaaK is required for proper
183 ligation of O-antigen to the core OS of LPS[55]. Indeed, LPS PAGE profiles support the finding that
184 O-antigen levels in the Δ*waaK* strain were reduced significantly, *i.e.*, to levels similar to those in
185 the O-antigen ligase-knockout cells (Δ*waaL*) (**Figure 3e**). Together, these results indicate that the
186 O-antigen extending from the core OS plays a crucial role in protecting *S. enterica* from T6SS-
187 mediated interbacterial antagonism.

188 O-antigens are hypervariable repeat polysaccharides that present heterogeneity and a wide
189 range of chain lengths, which determine the uniqueness of bacterial serotypes[56]. Previous studies
190 have demonstrated that chain length regulators, such as WzzB and FepE, determine O-antigen
191 length and degree of polymerization in *S. enterica*[57, 58]. Our LPS PAGE profiles indicate that WzzB
192 is responsible for producing long (L)-modal length O-antigen chains (16-35 sugar repeat units),
193 whereas FepE is responsible for very long (VL) ones (>100 sugar repeat units) (**Figure 3f**). To
194 better define the protective role of O-antigen in protecting against interbacterial antagonism, we
195 constructed Δ*wzzB* and Δ*fepE* strains and subjected them to competition assays against *E. cloacae*
196 carrying an active T6SS. Interestingly, only the Δ*wzzB* cells displayed significant competitive
197 defects, whereas Δ*fepE* cells showed wild-type levels of protection (**Figure 3g**). In addition, both

198 mutants showed comparable survival in competition with *E. cloacae* Δ*tssM* (**Supplementary**
199 **Figure 3f**). Therefore, our mutational analyses and LPS PAGE profiles indicate that L-modal O-
200 antigen is sufficient to protect *S. enterica* from T6SS intoxication.

201 However, our data do not exclude the possibility that VL-modal O-antigen in *S. enterica*
202 may also offer protection against T6SS-mediated attacks by *E. cloacae*. In wild-type *S. enterica*,
203 the VL-modal O-antigen is present at significantly lower levels than the L-modal O-antigen
204 (**Figure 3f**). We hypothesized that increasing the abundance of VL-modal O-antigen could enhance
205 the protective ability during interbacterial competition. To test this, we heterologously
206 overexpressed *fepE* in wild-type *S. enterica*, leading to elevated levels of VL-modal O-antigen[59]
207 (**Figure 3h**). Notably, we observed that cells with overproduction of VL-modal length O-antigen
208 exhibited enhanced protection during interbacterial competition compared to control cells
209 harboring an empty vector (**Figure 3i**). These finding suggest that in wild-type *S. enterica*, L-
210 modal O-antigen is sufficient to confer protection against T6SS intoxication. However, when
211 overproduced, VL-modal O-antigen can also play a protective role during interbacterial
212 competition.

213

214 **LPS-mediated Protection Against T6SS Attack Extends to Other Gram-negative Bacteria**

215 Though LPS structure varies among Gram-negative species[56, 60], we speculated that its
216 intrinsic protective capacity against T6SS could be broadly conserved. We tested this hypothesis
217 by examining the protective function of LPS from two distantly related model species,
218 Enterohemorrhagic *E. coli* (EHEC) and *Citrobacter rodentium*. We constructed LPS-deficient
219 strains (Δ*waaO*) of these species and then subjected them to pairwise competition assays against
220 *E. cloacae* with or without an active T6SS. Compared to the wild-type strain, LPS-deficient cells

221 presented significant competitive deficits when incubated with *E. cloacae* carrying a functional
222 T6SS (**Figure 3j** and **Supplementary Figure 4a**). Inactivation of the T6SS abrogated the fitness
223 defects of those variants in the competition assay, supporting the notion that LPS-mediated
224 protection against the T6SS is conserved beyond *S. enterica* (**Supplementary figure 4b**).

225 Next, we sought to determine if LPS also provide protection against T6SS-mediated attacks
226 from other antagonistic bacteria that secrete distinct sets of T6SS effectors. For this purpose, we
227 employed *Burkholderia thailandensis*, a species with a well-characterized T6SS, and conducted
228 competition assays with wild-type *S. enterica* and its LPS-deficient variant[61]. As expected, the
229 LPS-deficient strain displayed reduced protection when co-cultured with wild-type *B.*
230 *thailandensis*, but not with the Δ*tssM* strain (**Supplementary Figures 4c, d**). These results suggest
231 that the protective role of LPS against T6SS-mediated antagonism is widespread across bacterial
232 species and effective against diverse T6SS-bearing competitors.

233

234 **LPS-targeting Endoglycosidase in Phage Tail Spike Protein Increases Susceptibility to**
235 **Interbacterial Antagonism**

236 We have demonstrated herein that mutations in *S. enterica* genes involved in LPS
237 biosynthesis lead to increased susceptibility to T6SS-mediated attacks. Nevertheless, apart from
238 genetic variations in bacteria altering LPS structures, external stresses can also induce LPS
239 modifications, thereby compromising their protective capacity against antimicrobials from
240 predators and hosts, as well as environmental factors[62]. Consequently, we wanted to examine if
241 external stress-mediated LPS modification could influence the susceptibility of *S. enterica* during
242 interbacterial competition.

243 In our investigation into potential external modifiers of LPS, we found that many phages,
244 including our model phage P22, encode a dual-function tail spike protein (TSP) with LPS-targeting
245 endoglycosidase activity[63] (**Figure 4a** and **Supplementary Figure 1a**). This phage protein
246 mediates recognition of the bacterial host LPS receptor and hydrolyzes the O-antigen, allowing
247 phages to penetrate the bacterial cell envelope and inject their DNA upon viral infection[41, 64]
248 (**Figures 4b, c**). Notably, the TSP is highly active and stable under extreme conditions, making it
249 an ideal external agent to test our hypothesis without genetically manipulating *S. enterica*[65].
250 Consistent with previous reports, the TSP from phage P22 could be heterologously
251 expressed and affinity-purified in high amounts[66] (**Supplementary Figure 5a**). LPS PAGE
252 profiles indicated that wild-type TSP, but not the catalytic aspartate mutant TSP_{D392N}, degraded the
253 O-antigen of *S. enterica* (**Figure 4d**). Cells treated with TSP (wild-type or D392N) did not exhibit
254 detectable growth defects in monoculture (**Supplementary Figure 5b**), but phage titers were
255 dramatically reduced, indicating that TSP treatment prevents P22 from recognizing the LPS
256 receptor (**Figure 4e**). Next, we assessed if TSP-treated *S. enterica* exhibits increased susceptibility
257 to T6SS-mediated assaults. Indeed, TSP-treated cells showed reduced interbacterial
258 competitiveness when co-incubated with *E. cloacae* possessing an active T6SS compared to the
259 control experiment using either wild-type cells or cells treated with TSP_{D392N} (**Figure 4f**). The
260 resulting competitive fitness defect was similar to that observed for the LPS-deficient strain
261 (Δ*waaL*) (**Figure 4f**). Inactivation of the T6SS abrogated the fitness defects in TSP-treated cells
262 (**Figure 4g**). These results indicate that external LPS modifiers from phages, such as TSP with
263 endoglycosidase activity, can sensitize *S. enterica* to T6SS-mediated attacks.
264

265 **Phage-hosted Endoglycosidase Sensitizes *S. enterica* to Interbacterial Antagonism in Mixed**
266 **Populations**

267 Our data to this point support a model whereby the endoglycosidase activity of TSP cleaves
268 LPS O-antigen on bacterial cell surfaces, thereby sensitizing the bacteria to T6SS-mediated
269 assaults (**Figures 4f, g**). However, treating cells with concentrated, purified TSP might yield non-
270 physiologically relevant outcomes. In natural polymicrobial communities, TSP is anchored to the
271 phage tail baseplate during viral particle assembly[67], so the free form of TSP is likely present at
272 much lower concentrations than those used in our assays. Therefore, we investigated if the
273 presence of intact phage virions containing enzymatically active TSP could sensitize target bacteria
274 to interbacterial antagonism (**Figure 5a**).

275 Remarkably, when we incubated *S. enterica* with both phage P22 and *E. cloacae* carrying
276 an active T6SS, *S. enterica* survival significantly decreased (**Figure 5b**). The deficient fitness
277 phenotype was abolished when the T6SS of *E. cloacae* was inactivated or when *S. enterica* was
278 incubated with Felix O1 or Chi phages, which lack endoglycosidase activity in their tail spikes or
279 tail fibers[33, 68] (**Figures 5b, c**). These results corroborate our hypothesis that phages containing an
280 endoglycosidase targeting LPS sensitize host bacteria to T6SS-mediated attacks in mixed
281 microbial populations.

282 To validate this finding, we first ensured that *S. enterica* did not develop resistance to P22
283 during the phage-bacterium co-culture assay. Reinfecting surviving *S. enterica* with P22 resulted
284 in plaque titers comparable to those before the experiment, indicating that the competitive
285 phenotype was unlikely due to genetic adaptation (**Supplementary Figure 6a**). Next, we
286 confirmed that P22 does not cross-infect *E. cloacae*, as revealed by no P22 plaques being observed
287 even at a high plaque-forming unit (PFU) concentration using *E. cloacae* as the host

288 (**Supplementary Figure 6b**). To further minimize the impact of viral infection from different
289 phages, we subjected phages to 254 nm UV-C irradiation to crosslink their DNA, preventing DNA
290 injection into *S. enterica* while retaining the enzymatic activity of TSP in the tail spikes (**Figure**
291 **5d**). Strikingly, though phage titers decreased dramatically following UV treatment, the
292 competitive fitness deficits against the T6SS persisted in assays with *E. cloacae* and UV-treated
293 P22 (**Figures 5e-g**). Again, no detectable competitive fitness differences were observed when *S.*
294 *enterica* was incubated with UV-treated Felix O1 or Chi (**Figures 5f, g** and **Supplementary**
295 **Figures 6c, d**). Together, these outcomes indicate that phages with endoglycosidase activity in
296 their TSPs for binding and hydrolyzing LPS increase the susceptibility of *S. enterica* to
297 interbacterial antagonism in mixed microbial populations.
298

299 **Newly Isolated Environmental Phages That Sensitize *S. enterica* to Interbacterial**
300 **Antagonism**

301 We next sought to determine if the ability to sensitize *S. enterica* to interbacterial
302 antagonism is specific to the model phage P22 or if this trait is widespread in natural environments.
303 To investigate this, we isolated phages targeting *S. enterica* from soil samples collected in Northern
304 Taiwan. Four phages, designated As1 through As4, were successfully identified, each exhibiting
305 unique shapes and plaque morphologies (**Figure 5h** and **Supplementary Figure 6e**). These newly
306 isolated phages were then assessed for their impact on interbacterial competition.

307 Notably, two of the four phages, As1 and As3, both belonging to the family Podoviridae,
308 significantly reduced the competitiveness of *S. enterica* when co-incubated with *E. cloacae*
309 possessing an active T6SS, similar to the effect observed with phage P22 (**Figure 5i**). In contrast,
310 co-incubation with phages As2 or As4 did not affect the competitiveness of *S. enterica* (**Figure 5i**).

311 The competitiveness of *S. enterica* remained consistent across all groups when incubating with *E.*
312 *cloacae* lacked a functional T6SS (**Figure 5j**). Additionally, whole-genome sequencing of the
313 newly isolated phages As1 and As3 revealed the presence of *tsp* genes encoding predicted
314 endoglycosidases. These findings suggest that the ability of phages to sensitize bacteria to
315 interbacterial antagonism is prevalent in natural environments.
316

317 **Evidence that the O-antigen of LPS Serves as a Physical Barrier against Interacting Bacteria**

318 The LPS-containing outer membrane of Gram-negative species serves as a barrier against
319 various harmful agents, including hydrophobic antibiotics, antimicrobial peptides, detergents, and
320 bile acids[69, 70]. The structural complexity of LPS is critical for regulating membrane permeability,
321 which may be compromised by any modifications[71]. Previous studies have demonstrated that LPS
322 remodeling can alter the negative charge on the bacterial surface or affect the binding of divalent
323 cations, thereby impacting the stability of the outer membrane[72]. Therefore, one plausible
324 explanation for the observed interbacterial competitive defects displayed by our LPS O-antigen-
325 deficient variants is an increase in permeability of their outer membrane. To investigate this
326 possibility, we performed two standard outer membrane permeability assays: *i*) N-phenyl-1-
327 napthylamine (NPN) uptake; and *ii*) vancomycin (VAN) sensitivity. NPN is a hydrophobic
328 fluorescent probe that exhibits increased fluorescence upon interacting with the hydrophobic core
329 of a disrupted membrane, making it a reliable indicator of membrane permeability[73]. Vancomycin,
330 a glycopeptide antibiotic, is typically ineffective against Gram-negative bacteria due to its large
331 molecular size and inability to penetrate an intact outer membrane. However, its efficacy can
332 increase if membrane integrity is compromised[74]. Therefore, these assays can provide robust
333 measures of outer membrane permeability.

334 In the NPN uptake assay, we observed that wild-type cells pretreated with the metal
335 chelator ethylenediaminetetraacetic acid (EDTA) showed a significant increase in NPN
336 fluorescence, indicative of membrane disruption. However, no significant difference in NPN
337 uptake was observed between the wild-type cells and the O-antigen-deficient mutants (*i.e.,* Δ*wzzB*,
338 which lacks L-modal length O-antigen, and Δ*waaL* that lacks all O-antigens) (**Figure 6a**).
339 Similarly, in the VAN sensitivity assay, neither mutant strain demonstrated increased sensitivity to
340 vancomycin compared to the wild-type strain (**Figure 6b**). These results are in line with previous
341 studies on LPS in *E. coli*, which have shown that the core OS of LPS is particularly crucial for
342 maintaining outer membrane permeability[75]. As both the Δ*wzzB* and Δ*waaL* mutants preserve the
343 core OS structure, their increased susceptibility to T6SS-mediated attacks is unlikely to be
344 attributable to compromised outer membrane permeability.

345 Given that the T6SS punctures and injects toxins into interacting bacteria in a contact-
346 dependent manner[76], we next hypothesized that the O-antigen of LPS might act as a physical
347 barrier, partially hindering T6SS-mediated penetration by limiting close-range interaction. To test
348 this hypothesis, we immobilized *S. enterica* wild-type and O-antigen-deficient mutants on a mica
349 substrate and employed atomic force microscopy (AFM) to characterize bacterial surface
350 morphology[77] (**Figure 6c**). Interestingly, the resolved AFM images reveal distinct and clear
351 grooved structures on the surfaces of both the wild-type and Δ*wzzB* mutant (**Figures 6d, e**). In
352 contrast, the Δ*waaL* mutant, which retains only the core OS, displayed a more flattened surface
353 (**Figure 6f**). A similar groove-like surface morphology has been observed in other bacteria[78, 79],
354 and flattened cell surfaces have been noted in O-antigen-deficient cells[80].

355 To gain more insight into the mechanical properties of LPS, we further analyzed the force-
356 distance curves, which represent the interaction between the AFM tip and the bacterial surface

357 (**Figure 6g**). The force-distance profiles of both wild-type and mutant strains exhibited two distinct
358 force-slope changes, indicative of interactions with two different substrates (**Supplementary**
359 **Figure 7**). The first substrate corresponds to the LPS layer, and the second stiffer substrate
360 represents the outer membrane and cell wall (**Figure 6c**). For a more precise description, we
361 defined point 1 as the initial contact between the AFM tip and the LPS layer (x = 0, y = 0), and
362 point 2 as the transition point between the LPS layer and the outer membrane (**Figure 6g**). By
363 measuring the distance between points 1 and 2, we determined that LPS length in wild-type cells
364 is 5.39±1.16 nm, consistent with predictions for intact LPS structures (**Figure 6h**). In contrast,
365 Δ*wzzB* cells, which lack L-modal O-antigen, exhibited a reduced LPS length of 3.96±0.424 nm,
366 and Δ*waaL* cells that retain only the core OS had an LPS length of 3.39±0.41 nm (**Figures 6i, j**).
367 LPS length in wild-type cells was significantly more variable than in the mutants, implying
368 heterogeneity in LPS structure (**Figure 6k**). The loss of L-modal O-antigen in Δ*wzzB* led to a
369 marked reduction in the force region, similar to the reduction observed in the Δ*waaL* mutant
370 (**Figure 6k**). These LPS lengths are comparable to those reported in studies of *E. coli* strains with
371 the core OS but lacking O-antigen, for which LPS length was approximately 3±2 nm[78]. The
372 reduction in LPS length we determined for our O-antigen-deficient mutants indicates that the O-
373 antigen functions as a physical barrier, potentially hindering close interactions with competing
374 bacteria.
375

376 ## DISCUSSION

377 Bacterial integrity has been shaped over billions of years through interactions with other
378 microorganisms, with antagonistic interactions serving as a key driver of bacterial evolution and
379 physiology[7]. Extensive research has elucidated the diverse mechanisms bacteria employ to defend

380 themselves from biotic threats, highlighting their importance in the survival and adaptation of
381 bacterial species. Although these defensive adaptations offer clear evolutionary benefits, they are
382 not without fitness costs[18, 25]. Our results demonstrate that though modification of surface receptors
383 enables bacterial populations to effectively resist and adapt rapidly to phage infection, such
384 adaptation imposes significant fitness costs, increasing susceptibility to contact-dependent killing
385 by other antagonistic bacteria. These findings emphasize the fine balance between adaptation and
386 vulnerability in microbial interactions, suggesting that antagonistic coevolution plays a pivotal role
387 in shaping the dynamics of bacterial communities.

388 Our results reveal a hitherto unappreciated dual role for LPS as both a receptor for phage
389 adsorption and a protective barrier against close-contact bacterial competitors. Our observation
390 that T6SS-mediated interbacterial antagonism is more effective against LPS-deficient strains
391 implies a significant evolutionary trade-off, wherein resistance to phage predation may increase
392 susceptibility to other biotic threats. Furthermore, our results indicate that the protective function
393 of LPS against the T6SS is likely conserved across different Gram-negative bacteria, as evidenced
394 by the similar competitive fitness defects observed in LPS-deficient variants of *E. coli* and *C.*
395 *rodentium*. This evolutionary conservation points to broader ecological implications, with
396 modifications of the LPS potentially significantly influencing microbial community composition
397 across different populations.

398 The extent to which LPS protects against other contact-dependent killing mechanisms
399 beyond the T6SS remains unclear. For example, bacterial genera such as *Xanthomonas* and
400 *Stenotrophomonas* possess a Type IV Secretion System (T4SS) specialized in transferring toxic
401 effectors into neighboring cells in a contact-dependent manner, leading to cell death[81-83]. The
402 evidence presented in our study supports that LPS functions as a physical barrier, potentially

403 hindering close contact with interacting bacteria. Therefore, it is plausible that LPS might similarly
404 interfere with toxin delivery by other bacterial nanomachines, representing a broader defensive
405 strategy against diverse biotic threats.

406 Interestingly, our study has also revealed that phages can influence interbacterial
407 competition in ways beyond direct lysis. Specifically, phages with endoglycosidase activity in their
408 TSPs can degrade the O-antigen of target bacteria, thereby sensitizing them to interbacterial
409 antagonism. This scenario adds a new dimension to our understanding of phage-bacterial
410 interactions, whereby phages not only act as predators but also modulate bacterial interactions by
411 compromising the structural integrity of bacterial membranes. Notably, purified TSP, unlike whole
412 phage particles, do not promote resistant mutations as they do not directly kill bacteria[84]
413 (**Supplementary Figure 5b**). Our discovery reveals a plausible mechanism by which TSP
414 facilitates the clearance of target cells, with antagonistic bacteria that occupy the same ecological
415 niches potentially eliminating competitors more effectively when the LPS of those competitors is
416 cleaved by exogenous TSP[66].

417 We propose a working model of how phages may act as a key modulator of interbacterial
418 competition within bacterial communities (**Figure 7**). In the absence of phages, bacterial
419 competitors deploy specialized weaponry, such as the T6SS, to antagonize rivals and promote
420 niche partitioning. However, in the presence of phages, two distinct scenarios could alter this
421 dynamic: (1) bacteria may develop protective modifications on their surfaces to prevent phage
422 adsorption, reducing the likelihood of infection; or (2) phages equipped with LPS-targeting
423 endoglycosidases in their TSPs cleave the LPS of recipient cells. Both scenarios increase the
424 susceptibility of target cells to contact-dependent killing, facilitating niche invasion and leading to
425 the competitive exclusion of target populations. This phage-driven enhancement of bacterial

426 competition introduces a novel layer of complexity to microbial interactions, emphasizing the dual
427 evolutionary pressures imposed by both phage predation and bacterial antagonism. Our findings
428 underscore the critical role phages play in influencing bacterial competition and shaping microbial
429 community structure. The interplay between bacterial defense mechanisms and phage-mediated
430 pressures indicates that, beyond their traditional role as predators, phages may act as indirect
431 facilitators of interbacterial interactions. This model establishes a framework for future studies to
432 investigate these dynamics across diverse microbial ecosystems and environmental contexts,
433 which is essential for a comprehensive understanding of microbial ecology.

434 Further research should focus on how these interactions influence the long-term stability
435 and composition of bacterial populations in natural settings. In addition, the therapeutic potential
436 of phage-derived enzymes, such as TSP, should be explored in greater detail, particularly given the
437 growing global threat of antibiotic resistance. Phage-derived enzymes could offer a novel approach
438 to antimicrobial therapy by targeting bacterial defenses and enhancing the efficacy of conventional
439 treatment strategies[85].
440

441 # METHODS

442 **Bacteria, phages, and culture conditions**

443 The bacterial and phage strains used in this study are listed in Supplementary Table 1. The
444 following *Escherichia coli* strains were used: DH5α and PIR1 for cloning and plasmid
445 maintenance; S17-1 λ pir for conjugal transfer of the pRE118 plasmid into *S. enterica*, *E. coli*, and
446 *C. rodentium*; and BL21 (DE3) for overproduction and purification of TSP protein samples.
447 *Salmonella enterica* serovar Typhimurium ATCC-14028, *Enterobacter cloacae* ATCC-13047,
448 enterohemorrhagic *Escherichia coli* EDL933, *Citrobacter rodentium* DBS100, and *Burkholderia*
449 *thailandensis* E264 were used for bacterial co-culture and competition assays. Bacterial strains
450 were routinely grown in Luria Bertani (LB) medium or Brain Heart Infusion (BHI) medium with
451 appropriate antibiotics at 37 °C and shaking at 200 rpm. Antibiotics were used at the following
452 concentrations: 50 μg/mL for kanamycin, 25 μg/mL for chloramphenicol, 50 μg/mL for
453 streptomycin, 50 μg/mL for nalidixic acid, and 15 μg/mL for gentamycin.

454

455 **Plasmid construction**

456 All plasmids and primers used in our study are listed in Supplementary Table 1. In-frame
457 chromosomal deletions in *S. enterica*, *E. coli*, and *C. rodentium* were generated using the pRE118
458 vector[86]. To generate chromosomal mutation constructs, 800 bp regions flanking the mutation site
459 were amplified by polymerase chain reaction (PCR), sewn together, and inserted into the vector
460 using Gibson assembly at *XbaI* and *SacI* restriction sites[87]. For the expression and purification of
461 P22 TSP, the region encoding amino acid residues 109-666 was PCR-amplified and inserted into
462 pETDuet-1 with an N-terminal His^6-tag using Gibson assembly at the *BamHI* and *NotI* restriction
463 sites. The TSP catalytic mutant D392N was generated via site-directed mutagenesis[88]. To

464 overexpress *wzzB* and *fepE*, the respective genes were amplified by PCR and inserted into the
465 inducible pPSV39 vector via Gibson assembly at the *XbaI* and *SacI* restriction sites[89].
466
467 **Generation of mutant strains of *S. enterica*, *E. coli*, and *C. rodentium***
468 To generate deletions in *S. enterica*, *E. coli*, and *C. rodentium*, mutation constructs cloned
469 into pRE118 were transformed into conjugative *E. coli* S-17 λ pir[86]. Conjugative donor cells
470 carrying the deletion construct and recipient cells were grown overnight on LB plates containing
471 the appropriate antibiotics. The donor and recipient cells were then mixed at a 10:1 ratio, spotted
472 onto LB agar plates, and incubated at 37 °C for 6 hours to allow transfer of the deletion plasmid
473 via conjugation. The cell mixtures were scraped into LB medium and plated onto LB agar
474 supplemented with kanamycin and chloramphenicol (for *S. enterica* and *E. coli*) or kanamycin and
475 nalidixic acid (for *C. rodentium*) to select for cells containing the chromosomally inserted deletion
476 construct. The merodiploid strains were grown overnight in non-selective LB medium at 37 °C,
477 followed by counter-selection on nutrient agar supplemented with 10% (*w/v*) sucrose at room
478 temperature. Kanamycin-sensitive colonies were picked, and the deletions were confirmed by
479 colony PCR and Sanger sequencing. The chloramphenicol-resistant *S. enterica* and *E. coli* strains
480 were generated using pGRG37 methods[90].
481
482 **Phage propagation**
483 *S. enterica* ATCC-14028 was used as the host for phage propagation to obtain a high-titer
484 phage lysate (>10^8 PFU). An overnight culture was diluted in 50 mL of fresh LB broth to an OD_{600}
485 of 0.015 and incubated at 37 °C until the OD_{600} reached 0.2. Phage lysate was then added at a low
486 multiplicity of infection (MOI = 0.1), and the culture was incubated at 37 °C for 6 hours. After

487 incubation, the mixture was centrifuged at 6,000 x *g* for 10 minutes and filtered through a 0.2-µm
488 filter. The phage lysate was stored at 4 °C until use, and the phage titer was determined by spot
489 assays.
490
491 **Isolation of bacteriophage from soil**
492 Soil samples were collected from Nangang District in Taipei City. Each soil sample was
493 suspended in 50 mL of phage resuspension buffer (10 mM Tris-HCl, pH 7.5, 10 mM $MgSO_4$, 68.5
494 mM NaCl, 1 mM $CaCl_2$) and maintained on a rotator overnight to release the phage particles into
495 the buffer. The samples were centrifuged at 7,000 x g for 15 minutes at 4 °C, and the supernatants
496 were collected through 0.45-µm syringe filters.
497 For phage enrichment and single phage purification, 500 µL of host bacteria growing in
498 the early stationary phase was added to the samples along with fresh BHI medium. The samples
499 were supplemented with 10 mM $CaCl_2$ to enhance phage growth and incubated overnight at 37 °C,
500 shaking at 120 rpm. The enriched samples were then centrifuged at 13,000 x g for 15 minutes at 4
501 °C, and the supernatants were filtered through 0.45-µm syringe filters to obtain the phage
502 suspension. The double-layer agar method was then used to obtain single phage plaques. A single
503 plaque was selected and stored in BHI broth supplemented with 20% (*v/v*) glycerol at −80 °C.
504
505 **Spot assay**
506 To calculate the phage titer, 100 µL of mid-log phase *S. enterica* (OD_{600} = 0.5 – 0.8) was mixed
507 with either 4 mL of prewarmed 0.7% (*w/v*) soft LB agar or 8 mL of 0.5% (*w/v*) soft BHI agar and
508 immediately poured onto 1.5% (*w/v*) regular LB agar plates. Then, 2 µL of 10-fold serially diluted
509 phage lysate was spotted onto the bacterial lawn. The plates were allowed to dry at room

510 temperature and subsequently incubated at 37 °C overnight. The number of visible single plaques
511 in each spot was counted to calculate the phage titer.
512
513 **Transposon mutant library construction**
514 The *S. enterica* transposon mutant library was constructed as described previously, with
515 slight modifications[91]. In brief, *S. enterica* cultures were harvested at mid-log phase (OD_{600} = 0.5)
516 and gently washed with sterilized 10% (*w/v*) glycerol. The EZ-Tn5<KAN-2> Tnp transposome
517 complex (Epicentre BioTechnologies) was added to the electrocompetent cells, which were
518 incubated on ice for 10 minutes. The mixture was then transferred to an ice-cold 1-mm
519 electroporation cuvette and electroporated at 2,450 V. Pre-warmed SOC medium was added, and
520 the cells were allowed to recover at 37 °C for 90 minutes. Tn5 mutants were selected on LB agar
521 plates containing kanamycin, pooled, and stored in LB medium with 50% (*w/v*) glycerol at -80 °C.
522 Approximately 12,000 Tn5::KanR insertion mutants were collected.
523
524 **Isolation of phage-resistant variants**
525 The *S. enterica* transposon library was inoculated into fresh LB broth containing
526 kanamycin and incubated at 37 °C until the culture reached the early log phase (OD_{600} = 0.2).
527 Phage lysate containing 10^8 PFU was then added to the culture, which was incubated at 37 °C for
528 1 hour. The OD_{600} was monitored hourly until the culture reached mid-log phase (OD_{600} = 0.5).
529 Bacterial samples from the infected culture were plated on LB agar containing kanamycin and
530 incubated at 37 °C overnight. Colonies of *S. enterica* that grew on the plates were picked and tested
531 for phage resistance by spot assay. To confirm that the phage-resistant variants were not lysogens,

532 the putative phage-resistant cells were treated with mitomycin C and plated on an *S. enterica* lawn
533 for further analysis.
534
535 **Identification of phage-resistant mutations**
536 The workflow for identifying phage-resistant mutations is depicted in **Supplementary**
537 **Figure 2a**. Phage-resistant strains were grown in LB broth at 37 °C overnight, followed by
538 genomic DNA (gDNA) extraction using a DNeasy Blood & Tissue Kit (Qiagen). Primer extension
539 with single primer (EzTn_s) was performed to amplify a fragment of the Tn5-gDNA junction. The
540 extension cycle included a manual hot start, with initial denaturation at 95 °C for 2 minutes,
541 followed by the addition of polymerase. The linear extension products were purified using
542 SPRIselect Bead-Based Reagent (Beckman Coulter). A deoxycytidine homopolymer tail (C-tail)
543 was added to the 3' end of the linear extension products using terminal deoxynucleotidyl
544 transferase (TdT; New England Biolabs). The reaction was carried out at 37 °C for 1 hour, followed
545 by enzyme inactivation at 75 °C for 20 minutes. The C-tailed products were then purified again
546 using SPRIselect Bead-Based Reagent. The purified C-tailed products were enriched by PCR using
547 Tn5_F and Tn5_R primers. Finally, the PCR products were heated at 65 °C for 15 minutes and
548 analyzed on 1.5% agarose gels. DNA fragments ranging from 300 to 500 bp were gel extracted for
549 Sanger sequencing and BLAST analysis.
550
551 **Monoculture bacterial growth in LB broth**
552 Bacteria were cultured overnight and subsequently diluted to an OD_{600} of 0.1 in LB broth.
553 A total of 100 μL of the diluted cells was transferred to 96-well, clear-bottom microplates, and the
554 growth rate was measured every 10 minutes for 12 hours using an Infinite F200 series plate reader

555 (Tecan). To prevent cell aggregation, 10 seconds of shaking was applied prior to each measurement.
556 Blank media and the wild-type strain were included on each plate, and at least three biological
557 replicates were measured for each sample.
558
559 **Monoculture bacterial growth on solid agar**
560 Overnight cultures grown in LB medium were pelleted, washed, and adjusted to an OD_{600}
561 = 20. Cell mixture (5 μL) was spotted onto nitrocellulose filters placed on LB agar plates and
562 incubated at 37 °C for 12 hours. Cells were then scraped from the nitrocellulose and resuspended
563 in 200 μL of LB broth. Initial and post-co-culture cell counts were determined by performing 10-
564 fold serial dilutions and plating the dilutions on LB agar plates containing the appropriate antibiotic.
565
566 **LPS analysis**
567 LPS was analyzed as previously described, with some modifications[92]. In brief, overnight
568 bacterial culture (OD_{600} = 10) was pelleted and resuspended in 150 μL of Dissociation Buffer A
569 (0.5 M Tris-HCl pH 6.8, 10% (*w/v*) glycerol, 10% (*w/v*) SDS, 5% (*v/v*) β-mercaptoethanol),
570 followed by boiling for 10 minutes. After cooling to room temperature, the samples were
571 centrifuged at 18,000 x *g* for 15 minutes. The supernatant (100 μL) was diluted into 900 μL of
572 Dissociation Buffer B (0.5 M Tris-HCl pH 6.8, 10% (*w/v*) glycerol, 0.05% (w/v) bromophenol
573 blue) supplemented with 1 μL of 20 mg/mL proteinase K, and incubated at 37 °C for 1 hour. The
574 samples were separated on 12% or 20% (*w/v*) SDS-PAGE and stained using a Pro-Q Emerald 300
575 Lipopolysaccharide Gel Stain Kit (Invitrogen) for imaging.
576
577 **Transmission Electron Microscopy (TEM) analysis**

578 For TEM analysis, 4 μL droplets of phage lysate (~10^{10} PFU/mL) were placed on copper
579 grids (300 mesh) coated with a carbon-coated formvar film (Ted Pella Inc., Redding, CA). The
580 phage lysate was allowed to settle for 1 minute at room temperature and then dried using 3M filter
581 paper. Negative staining was performed with 1% (*w/v*) uranyl acetate for 30 seconds, after which
582 the excess stain was removed with 3M filter paper. The sample was gently washed three times with
583 sterilized distilled deionized water, and the grid was air-dried overnight at room temperature.
584 Phage morphology was visualized using a Talos 120 C transmission electron microscope (Thermo,
585 Waltham, US).
586
587 **Bacterial co-culture experiments**
588 Overnight cultures grown in LB medium were pelleted, washed, and adjusted to an OD_{600}
589 of 5 for liquid co-culture assays or to an OD_{600} of 20 for assays on solid agar. Cells were mixed at
590 a 1:1 ratio in LB broth and incubated at 37 °C for 1 hour. For solid agar experiments, 5 μL of the
591 cell mixture was spotted onto nitrocellulose filters placed on LB agar plates and incubated at 37
592 °C for 3 hours. Cells were then scraped from the nitrocellulose and resuspended in 200 μL of LB
593 broth. Initial and post-co-culture cell counts were determined by performing 10-fold serial
594 dilutions and plating the dilutions on LB agar plates containing the appropriate antibiotics. Relative
595 survival of the bacteria was calculated as the ratio of post-co-culture colony forming units (CFUs)
596 to the average CFUs of wild-type *S. enterica*.
597
598 **Macroscopic cell aggregation assay**
599 Macroscopic cell aggregation assays were performed as described previously, with slight
600 modifications[93]. Bacterial cultures were grown overnight at 37 °C in LB broth containing

601 kanamycin. After incubation, the cultures were vortexed and transferred to a 2-mm cuvette. The
602 bacterial cultures were then allowed to settle at room temperature for 22 hours to observe cell
603 aggregation.
604
605 **Bacterial competition assays**
606 Competition assays were performed as described previously, with slight modifications[94].
607 The bacterial strains used in the assays were cultured overnight at 37 °C, harvested by
608 centrifugation, washed, and resuspended in LB medium. *E. cloacae* or *B. thailandensis* were used
609 as the donor strains, whereas *S. enterica*, *E. coli*, and *C. rodentium* served as the recipient strains.
610 Donor and recipient cells were mixed at a 10:1 ratio, and a 5 μL aliquot of the mixture was spotted
611 onto nitrocellulose filters placed on pre-warmed LB agar plates and incubated at 37 °C for 1 hour.
612 For assays involving *wzzB* or *fepE* overexpression strains, the mixtures were spotted on LB agar
613 plates supplemented with 0.5 mM IPTG. Following incubation, cells were scraped from the
614 nitrocellulose filters, resuspended in 200 μL of LB broth, and serially diluted (10-fold) for CFU
615 counting on LB agar plates with appropriate antibiotics. The bacterial relative protective index was
616 calculated as the ratio of the output recipient-to-donor ratio divided by the input recipient-to-donor
617 ratio, followed by normalization to the protective index of wild-type *S. enterica*.
618 To investigate the effect of phage-derived LPS modifiers on bacterial susceptibility to
619 T6SS-mediated attacks, wild-type *S. enterica* cells were treated with purified TSP (10 nM), live
620 phages (10^5 PFU/mL), or UV-inactivated phages (10^5 PFU/mL) for 10 minutes at 37 °C. Treated
621 cells were then mixed with *E. cloacae* at a 10:1 donor-to-recipient ratio, and the mixture was
622 spotted onto nitrocellulose filters placed on pre-warmed LB agar plates. After incubation at 37 °C
623 for 1 hour, cells were collected by scraping them from the filters and resuspending them in 200 μL

624 of LB broth. Initial and post-co-culture CFU counts were determined through serial dilutions and
625 plating on LB agar with selective antibiotics. The bacterial relative protective index was calculated
626 as the ratio of the output recipient-to-donor ratio divided by the input recipient-to-donor ratio and
627 normalized to the protective index of wild-type *S. enterica*.
628
629 **P22 TSP purification**
630 Purification of recombinant P22 TSP (wild-type and D392N mutant) was performed as
631 described previously[95]. In brief, the N-terminal His^6-tagged TSP was expressed in *E. coli* BL21
632 (DE3). An overnight culture was diluted 100-fold into 1 L of LB medium containing carbenicillin
633 and incubated at 37 °C until the culture reached mid-log phase (OD_{600} = 0.6 - 0.8). TSP expression
634 was induced by adding 1 mM IPTG and incubating at 37 °C for 4 hours. Cells were harvested by
635 centrifugation at 4 °C and resuspended in 20 mL of resuspension buffer (20 mM Tris-HCl pH 7.5,
636 300 mM NaCl, 5 mM imidazole pH 7.0, 1 mM DTT, and a protease inhibitor cocktail). The
637 resuspended cells were disrupted by sonication, and cell debris was removed by centrifugation at
638 40,000 × *g* for 30 minutes at 4 °C. The soluble His^6-TSP was purified from the supernatant using
639 gravity flow through a 2 mL Ni-NTA agarose column. Bound proteins were eluted using a linear
640 imidazole gradient (25 to 300 mM). Purified proteins were analyzed by 12.5% (*w/v*) SDS-PAGE
641 followed by Coomassie Brilliant Blue staining.
642
643 **Phage inactivation by UV treatment**
644 The purified phage stock was diluted to ~10^9 PFU/mL, and 1 mL aliquots were placed in
645 Petri dishes covered with parafilm. The dishes were exposed to 254 nm UV light using a
646 Stratalinker UV Crosslinker 1800 (Stratagene, La Jolla, CA) for the indicated time intervals. Phage

647 infection efficiency following UV treatment was assessed by spot assay (**Figure 5e,** and
648 **Supplementary Figures 6c, d**).
649
650 **Membrane permeability assays**
651 Outer membrane permeability was assessed using NPN uptake and VAN sensitivity assays,
652 as described previously[73, 96]. For the NPN uptake assay, mid-log phase cultures (OD_{600} = 0.5) were
653 pelleted and gently washed with 5 mM HEPES buffer (pH 7.2). An equal volume of HEPES buffer
654 containing 20 μM NPN was added to the samples and mixed thoroughly. As a control, 1 mM EDTA
655 was added to wild-type cells. Fluorescence was measured using an optical-bottom black plate in a
656 SpectraMax iD5 microplate reader (Molecular Devices) with excitation at 350 nm and emission at
657 420 nm, recorded at 30-second intervals for 10 minutes. Data collected over 10 minutes were
658 averaged, and NPN uptake activity was normalized by subtracting the background fluorescence in
659 the absence of NPN. For the VAN sensitivity assay, overnight cultures were diluted to an OD_{600} of
660 0.05 in 25 mL of LB broth, followed by the addition of 150 μg/mL vancomycin. As a control, 1
661 mM EDTA was added to wild-type cells. After 2 hours of incubation at 37 °C, CFUs were
662 determined by performing 10-fold serial dilutions and plating on LB agar.
663
664 **Atomic force microscopy (AFM)**
665 Atomic force microscopy sample preparation was performed as described previously, with
666 some modifications[97]. An overnight bacterial culture was diluted 100-fold and incubated at 37 °C
667 until it reached mid-log phase (OD_{600} = 0.6 – 0.8). Cells were harvested by centrifugation at OD_{600}
668 = 1, washed, and then resuspended in 10 mM HEPES buffer (pH 7.4)[98]. For immobilization, 200
669 μL of the bacterial suspension was applied to freshly cleaved mica and incubated for 20 minutes

670 at room temperature. Following immobilization, the sample was gently rinsed with Milli-Q water
671 to remove any non-adherent cells, then air-dried in a desiccator for 30 minutes prior to AFM
672 measurements.

673 AFM measurements were carried out using a Multimode NanoScope V system (Bruker
674 AXS) with PeakForce Tapping (PFT) and Force Volume (FV) mapping modes. A commercial tip
675 holder equipped with silicon (Si) cantilevers (FMAuD, NanoSensor), a spring constant of 2.0 N/m,
676 and a resonance frequency of 70.0 kHz was employed. PFT mode was used for high-resolution
677 imaging with a peak force setpoint of 1 nN and modulation of 2 kHz in the Z-ramp. For mechanical
678 mapping and force spectroscopy, FV mode was employed to collect force-distance (F-Z) curves
679 across the sample surface. Force spectroscopy was conducted using 32 × 32 pixels in the XY scan
680 area with 512 points per force curve at a 3 Hz Z-ramp for data acquisition and analysis. The force-
681 distance curves were calibrated from the original force-displacement (F-D) data following standard
682 processing protocols[99]. AFM imaging was restricted to isolated bacterial cells to prevent
683 confounding effects from cell aggregation. The AFM instrument was housed in a humidity-
684 controlled environment (~35%) to reduce capillary forces between the AFM tip and the bacterial
685 surface. Raw AFM images were processed and analyzed using Nanoscope Analysis software
686 (Bruker AXS).

687 To analyze force-distance curves, the initial jump-in force (point 1) was defined as the
688 contact point on the LPS layer, corresponding to a tip-sample distance of 0 nm and a tip-sample
689 interaction force of 0 nN. Two distinct interaction profiles from each force curve were identified
690 by slope changes, in which the increase of the slope represented contact with a stiffer substrate.
691 The length of the LPS layer was measured as the distance between point 1 and point 2 (**Figure 6g**).

692 Ten force curves were obtained from multiple cells at different locations to ensure representative
693 sampling.
694
695 **Quantification and statistical analysis**
696 Statistical significance in bacterial co-culture and competition assays was assessed by
697 unpaired two-tailed t-tests between relevant samples. Statistical significance are provided in the
698 figure legends.
699

700 ## ACKNOWLEDGMENTS

701 We thank Dr. Waldemar Vollmer, Dr. Marcin Grabowicz, Dr. Harmit Malik, Dr. Meng-
702 Chiao Ho, and Ting laboratory members for helpful discussions; Dr. Joseph Mougous, Dr. Shu-
703 Jung Chang, Dr. Hsin-Hung Chou, Dr. Hung-Ta Chen, and Dr. Sue Lin-Chao for sharing reagents;
704 Dr. Soo-Chen Cheng and Dr. Jun-Yi Leu for sharing equipment; Dr. Shu-Yun Tung, Dr. Hsin-Nan
705 Lin, Dr. Chen-Hsin Yu, Ms. Wen-Li Pon, and Ms. Shin-Yi Du for technical assistance; and Dr.
706 John O'Brien for manuscript editing. We acknowledge funding support from Academia Sinica
707 (AS-CDA-112-L05 to S.-Y.T.) and the National Science and Technology Council, Taiwan (111-
708 2311-B-001-006-MY2, 112-2311-B-001-020, and 113-2628-B-001-008-MY3 to S.-Y.T.).
709

710 ## COMPETING INTERESTS

711 The authors declare no competing interests.
712
713
714

715 # FIGURE LEGENDS

716 **Figure 1. Isolation of phage-resistant *S. enterica* for pairwise co-culture experiments. (a)**
717 Schematic workflow for isolating phage-resistant strains from a transposon library (Tn-library)
718 pool containing approximately 12,000 mutants. Detailed procedures are provided in the Methods
719 section. Phages from different families of Caudovirales were used for selection: Felix O1, P22,
720 and Chi (**Supplementary Figure 1a**). Spot assays were employed to validate the resistance of the
721 isolated strains to phage infections (**Supplementary Figure 1b**). Validated resistant variants were
722 subsequently co-cultured with *E. coli* or *E. cloacae* in liquid broth or on solid agar. The survival
723 of *S. enterica* was quantified by counting CFUs on selective media. **(b, c)** Relative survival of the
724 indicated *S. enterica* strains compared to wild-type *S. enterica* grown in co-culture with *E. coli* or
725 *E. cloacae* in LB broth **(b)** or solid agar **(c)**. Relative survival was determined by comparing CFU
726 ratios of phage-resistant variants and the wild-type control. Data in **(b)** and **(c)** are represented as
727 means ± SD (n=6). Asterisks indicate statistically significant differences between the survival of a
728 mutant strain and the wild-type control ($p < 0.05$).

729

730 **Figure 2. Phage-resistant strains exhibit LPS deficiency and increased susceptibility to T6SS-**
731 **mediated antagonism by *E. cloacae*. (a, b)** 12% LPS PAGE profiles showing the levels of LPS
732 produced by the indicated *S. enterica* strains: **(a)** LPS from the Felix O1-resistant strains; **(b)** LPS
733 from the P22-resistant strains. A schematic representation of LPS is shown on the left. **(c-h)**
734 Protectiveness of the indicated *S. enterica* phage-resistant strains relative to the wild-type strain
735 after competition with *E. cloacae* wild-type **(c, d)**, Δ*tssM* **(e, f)**, and Δ*cdiA* **(g, h)** strains. Data in
736 **(c-h)** are presented as means ± SD (n=6). Asterisks indicate statistically significant differences
737 between the relative protective index of a mutant strain and the wild-type control ($p < 0.05$).

738

739 **Figure 3. LPS protects bacteria from T6SS-mediated assaults. (a)** Schematic representation of
740 the LPS structure in *S. enterica*. Glycosyltransferases involved in LPS biosynthesis are indicated.
741 **(b, d, g, i)** Protectiveness of the indicated *S. enterica* mutant or indicated protein overexpressing
742 strains relative to the wild-type strain after competition with wild-type *E. cloacae*. **(c, e, f, h)** LPS
743 PAGE profiles: **(c)** 20% gel; **(e, f, h)** 12% gel, showing LPS levels produced by the indicated *S.*
744 *enterica* mutant or indicated protein overexpressing strains. EV, empty vector. **(j)** Protectiveness
745 of the indicated bacterial species (Δ*waaO* mutant) relative to the wild-type strain after competition
746 with wild-type *E. cloacae*. Data in **(b, d, g, i, j)** are presented as means ± SD (n=6). Asterisks
747 indicate statistically significant differences between the relative protective index of a mutant strain
748 and the wild-type control ($p < 0.05$).

749

750 **Figure 4. Purified TSP increases the susceptibility of *S. enterica* to T6SS-mediated**
751 **intoxication. (a)** Schematic illustration of phage P22. **(b)** Crystal structure of the P22 TSP (PBD:
752 1TYX)[100] with the O-antigen substrate bound in the catalytic pocket. The D392 residue is
753 highlighted in pink. **(c)** Schematic representation of O-antigen digestion by phage P22 hosting an
754 enzymatically active TSP. **(d)** 12% LPS PAGE profiles showing LPS levels from wild-type *S.*
755 *enterica* treated with different concentrations of purified TSP (wild-type or D392N mutant) for 10
756 minutes at room temperature. LPS extracted from the Δ*waaL* strain is shown as a control. **(e)** Ten-
757 fold serial dilution spot assay of P22 phage on wild-type *S. enterica* treated with 10 nM purified
758 TSP. The image is representative of triplicate experiments. **(f, g)** Protectiveness of the wild-type *S.*
759 *enterica* strain treated with purified TSP (wild-type or D392N mutant) relative to the mock-treated
760 *S. enterica* after competition with *E. cloacae* wild-type **(f)** or Δ*tssM* **(g)** strains. Data in **(f, g)** are

761 presented as means ± SD (n=6). Asterisks indicate statistically significant differences between the
762 relative protective index of TSP-treated *S. enterica* and the mock-treated control ($p < 0.05$).
763
764 **Figure 5. Phage P22 sensitizes *S. enterica* to T6SS-mediated attacks in mixed populations. (a)**
765 Schematic representation of phages with or without LPS-targeting endoglycosidase during
766 infection of *S. enterica*. *E. cloacae* carrying a functional T6SS is depicted at the top. **(b, c)**
767 Protectiveness of the wild-type *S. enterica* strain treated with different phages (Felix O1, P22, or
768 Chi) relative to the mock-treated *S. enterica* after competition with *E. cloacae* wild-type **(b)** or
769 Δ*tssM* **(c)** strains. **(d)** Schematic of P22 with UV_{254nm} treatment. **(e)** Ten-fold serial dilution spot
770 assay of UV-inactivated P22 phage on wild-type *S. enterica*. The image is representative of
771 triplicate experiments. **(f, g)** Protectiveness of the wild-type *S. enterica* strain treated with UV-
772 inactivated phage particles (Felix O1, P22, or Chi) relative to the mock-treated *S. enterica* after
773 competition with *E. cloacae* wild-type **(f)** or Δ*tssM* **(g)** strains. **(h)** Ten-fold serial dilution spot
774 assay of phages As1, As2, As3, and As4. **(i, j)** Protectiveness of the wild-type *S. enterica* strain
775 treated with different phages (P22, As1, As2, As3, or As4) relative to the mock-treated S. enterica
776 after competition with *E. cloacae* wild-type **(i)** or Δ*tssM* **(j)** strains. Data in **(b, c, f, g, i, j)** are
777 presented as means ± SD (n=6). Asterisks indicate statistically significant differences between the
778 relative protective index of phage-treated or UV-inactivated phage-treated *S. enterica* and the
779 mock-treated control ($p < 0.05$).
780
781 **Figure 6. Evidence that the O-antigen of LPS serves as a physical barrier. (a, b)** Measurements
782 of outer membrane permeability of the *S. enterica* wild-type, Δ*wzzB*, and Δ*waaL* strains. EDTA (1
783 mM) was added to the wild-type as the control. **(a)** NPN uptake assay; **(b)** VAN sensitivity assay.

784 **(c)** Schematic representation of the atomic force microscopy (AFM) setup. *S. enterica* cells were
785 immobilized on freshly prepared mica substrates. A laser beam reflected on the back of the
786 cantilever is used to measure the force interactions between the probe and sample. The feedback
787 control system between the photodetector and the X-Y-Z scanner enables precise detection of the
788 surface morphology of the cells. A zoomed-in view of AFM measurement of the bacterial surface
789 is also shown. **(d-f)** Images of AFM height for the *S. enterica* wild-type **(d)**, Δ*wzzB* **(e)**, and Δ*waaL*
790 **(f)** strains, as obtained using the PeakForce Tapping (PFT) mode. The image scan size is 1 µm x 1
791 µm. **(g)** Schematic of the AFM force-distance curve obtained from *S. enterica* samples using the
792 Force Volume (FV) mapping mode. The point at which the tip contacts the sample is defined as
793 zero (point 1), and slope changes indicate a transition to a stiffer substrate (point 2). **(h-j)** Force-
794 distance curves for the *S. enterica* wild-type **(h)**, Δ*wzzB* **(i)**, and Δ*waaL* **(j)** strains. Ten curves were
795 captured from each sample at randomly selected locations, with the longest and shortest LPS
796 lengths highlighted. Red arrows mark points 1 and 2. **(k)** LPS length of the *S. enterica* wild-type,
797 Δ*wzzB*, and Δ*waaL* strains was determined from force-distance curves by measuring the distance
798 between point 1 and point 2.
799
800 **Figure 7. Working model of how phages modulate interbacterial competition within**
801 **microbial communities.** Bacterial interactions are shaped either by the absence (left) or presence
802 (right) of phages. **(a)** Bacteria inhabit polymorphic environments. **(b)** In the presence of P22 phage,
803 bacterial surfaces can be modified via two distinct mechanisms. **(c)** LPS-modified strains are
804 selected due to their resistance to phage adsorption, leading to their dominance within *S. enterica*
805 populations. **(d)** TSP from P22 phage specifically cleaves the bacterial O-antigen of LPS, resulting
806 in a shortened structure. **(e)** LPS deficiency increases the susceptibility of *S. enterica* to contact-

807 dependent killing by bacterial competitors in close proximity. **(f)** Phage-mediated surface
808 modifications influence the outcome of interbacterial competition, driving dynamic shifts in mixed
809 bacterial populations.
810
811 **Figure S1. Validation of phage resistance in isolated mutants and monocultural growth**
812 **experiments. (a)** TEM images of model phages used in the study: Felix O1 (left), P22 (middle),
813 and Chi (right). Scale bar = 0.1 μm. **(b)** Ten-fold serial dilution spot assay of phages Felix O1 (left),
814 P22 (middle), and Chi (right) on the indicated phage-resistant *S. enterica* strains. The image is
815 representative of triplicate experiments. **(c)** Growth curves of the indicated phage-resistant *S.*
816 *enterica* strains in LB broth at 37 °C. Wild-type, Δ*waaL*, and Δ*waaG* strains are shown as controls.
817 **(d)** CFUs of the indicated phage-resistant *S. enterica* strains grown at 37 °C for 12 hours on LB
818 agar plates. Wild-type, Δ*waaL* (ΔL), and Δ*waaG* (ΔG) strains are shown as controls.
819
820 **Figure S2. Characterization of transposon insertion mutations in phage-resistant *S. enterica***
821 **isolates. (a)** Schematic workflow for identifying phage-resistant mutations. Detailed procedures
822 are provided in the Methods section. **(b)** Mutated genes in the P22-resistant and Felix O1-resistant
823 *S. enterica* isolates. Scale bar = 500 bp. **(c)** Mutated genes in the Chi-resistant *S. enterica* isolates.
824 Scale bar = 1000 bp. **(d)** 12% LPS PAGE profiles showing LPS levels from the indicated Chi-
825 resistant *S. enterica* strains. A schematic representation of LPS is shown on the left. **(e, f)**
826 Macroscopic aggregation analysis to assess LPS deficiency in the indicated Felix O1-resistant **(e)**
827 or P22-resistant **(f)** *S. enterica* strains. The images are representative of triplicate experiments.
828

829 **Figure S3. LPS-deficient *S. enterica* mutants exhibit no significant growth or competition**
830 **defects. (a-c)** Growth curves of the indicated *S. enterica* LPS mutants in LB broth at 37 °C. The
831 wild-type strain is shown as a control. **(d-f)** Protectiveness of the indicated *S. enterica* mutant
832 strains relative to the wild-type strain after competition with *E. cloacae* Δ*tssM*. Data in **(d-f)** are
833 presented as means ± SD (n=6).
834
835 **Figure S4. LPS-deficient bacteria exhibit fitness deficits in competition with antagonistic**
836 **bacteria carrying active T6SS. (a)** 12% LPS PAGE profile displaying LPS levels produced by
837 the indicated *S. enterica*, *E. coli*, and *C. rodentium* strains. **(b)** Protectiveness of the indicated
838 bacterial species (Δ*waaO* mutant) relative to the wild-type strain after competition with *E. cloacae*
839 Δ*tssM*. **(c, d)** Protectiveness of the indicated bacterial species (Δ*waaO* mutant) relative to the wild-
840 type strain after competition with *B. thailandensis* wild-type **(c)** or Δ*tssM* **(d)** strains. Data in **(b-**
841 **d)** are presented as means ± SD (n=6). Asterisks indicate statistically significant differences in the
842 relative protective index between the mutant and wild-type strains ($p < 0.05$).
843
844 **Figure S5. TSP-treated *S. enterica* shows no significant growth defect. (a)** Coomassie-stained
845 12.5% SDS-PAGE analysis of the purified TSP (left) and the D392N catalytic mutant (right). **(b)**
846 Growth curves of wild-type *S. enterica* incubated with 10 nM of purified TSP (wild-type or D392N
847 mutant) at 37 °C. Mock-treated wild-type *S. enterica* and the Δ*waaL* mutant are shown as controls.
848
849 **Figure S6. Supporting evidence that phage P22 sensitizes *S. enterica* to T6SS-mediated**
850 **attacks. (a)** Ten-fold serial dilution spot assay of phages Felix O1 (left), P22 (middle), and Chi
851 (right) on wild-type *S. enterica* before and after the competition assay (**Figure 5b**). **(b)** Ten-fold

852 serial dilution spot assay of phages Felix O1 (left), P22 (middle), and Chi (right) on wild-type *S.*
853 *enterica* and *E. cloacae.* **(c, d)** Ten-fold serial dilution spot assay of UV-inactivated Felix O1 phage
854 **(c)** or Chi phage **(d)** on wild-type *S. enterica*. The images are representative of triplicate
855 experiments. **(e)** TEM images of isolated phages used in the study: As1 (top left), As2 (top right),
856 As3 (bottom left), and As4 (bottom right). Scale bar = 0.1 μm.
857
858 **Figure S7. The slope of AFM force-distance curves.** Two distinct slopes from each force-
859 distance curve were obtained for the *S. enterica* wild-type, Δ*wzzB*, and Δ*waaL* strains. Ten curves
860 were divided into two segments by point 2, as shown in **Figure 6g**. The slope measured from the
861 first segment corresponds to the LPS layer (left), whereas the second segment represents the outer
862 membrane (right).
863
864 **Supplementary Table 1.** Strains, Recombinant DNA, and Oligonucleotides used in this study.
865

866 # AUTHOR CONTRIBUTIONS

867 C.-E.T., F.-Q.W., C.-W.Y., I.-S.H., P.-Y.C., and S.-Y.T. designed the study. C.-E.T., F.-Q.W.,
868 C.-W.Y., L.-L.Y., Y.-C.C., and T.V.N. performed experiments. C.-E.T., F.-Q.W., C.-W.Y., I.-S.H.,
869 and S.-Y.T. analyzed data. C.-E.T., F.-Q.W., C.-W.Y., P.-Y.C., I.-S.H., and S.-Y.T. wrote the
870 manuscript.
871

872 # REFERENCES

873 1. Brussow, H. & Hendrix, R.W. Phage genomics: small is beautiful. *Cell* **108**, 13-16 (2002).
874 2. Garcia-Bayona, L. & Comstock, L.E. Bacterial antagonism in host-associated microbial
875 communities. *Science* **361** (2018).

3. Cotter, P.D., Ross, R.P. & Hill, C. Bacteriocins - a viable alternative to antibiotics? *Nat Rev Microbiol* **11**, 95-105 (2013).
4. Klein, T.A., Ahmad, S. & Whitney, J.C. Contact-Dependent Interbacterial Antagonism Mediated by Protein Secretion Machines. *Trends Microbiol* **28**, 387-400 (2020).
5. Chassaing, B. & Cascales, E. Antibacterial Weapons: Targeted Destruction in the Microbiota. *Trends Microbiol* **26**, 329-338 (2018).
6. Hoque, M.M., Espinoza-Vergara, G. & McDougald, D. Protozoan predation as a driver of diversity and virulence in bacterial biofilms. *FEMS Microbiol Rev* **47** (2023).
7. Smith, W.P.J., Wucher, B.R., Nadell, C.D. & Foster, K.R. Bacterial defences: mechanisms, evolution and antimicrobial resistance. *Nat Rev Microbiol* **21**, 519-534 (2023).
8. Murtazalieva, K., Mu, A., Petrovskaya, A. & Finn, R.D. The growing repertoire of phage anti-defence systems. *Trends Microbiol* (2024).
9. Kulikov, E.E., Golomidova, A.K., Prokhorov, N.S., Ivanov, P.A. & Letarov, A.V. High-throughput LPS profiling as a tool for revealing of bacteriophage infection strategies. *Sci Rep* **9**, 2958 (2019).
10. Kaur, G., Agarwal, R. & Sharma, R.K. Bacteriophage Therapy for Critical and High-Priority Antibiotic-Resistant Bacteria and Phage Cocktail-Antibiotic Formulation Perspective. *Food Environ Virol* **13**, 433-446 (2021).
11. Doron, S. *et al.* Systematic discovery of antiphage defense systems in the microbial pangenome. *Science* **359** (2018).
12. Vassallo, C.N., Doering, C.R., Littlehale, M.L., Teodoro, G.I.C. & Laub, M.T. A functional selection reveals previously undetected anti-phage defence systems in the E. coli pangenome. *Nat Microbiol* **7**, 1568-1579 (2022).
13. Kennedy, N.W. & Comstock, L.E. Mechanisms of bacterial immunity, protection, and survival during interbacterial warfare. *Cell Host Microbe* **32**, 794-803 (2024).
14. Peterson, S.B., Bertolli, S.K. & Mougous, J.D. The Central Role of Interbacterial Antagonism in Bacterial Life. *Curr Biol* **30**, R1203-R1214 (2020).
15. Hersch, S.J. *et al.* Envelope stress responses defend against type six secretion system attacks independently of immunity proteins. *Nat Microbiol* **5**, 706-714 (2020).
16. Cornforth, D.M. & Foster, K.R. Competition sensing: the social side of bacterial stress responses. *Nat Rev Microbiol* **11**, 285-293 (2013).
17. LeRoux, M., Peterson, S.B. & Mougous, J.D. Bacterial danger sensing. *J Mol Biol* **427**, 3744-3753 (2015).
18. Mangalea, M.R. & Duerkop, B.A. Fitness Trade-Offs Resulting from Bacteriophage Resistance Potentiate Synergistic Antibacterial Strategies. *Infect Immun* **88** (2020).
19. Chan, B.K. *et al.* Phage selection restores antibiotic sensitivity in MDR Pseudomonas aeruginosa. *Sci Rep* **6**, 26717 (2016).
20. Levin, B.R. & Bull, J.J. Population and evolutionary dynamics of phage therapy. *Nat Rev Microbiol* **2**, 166-173 (2004).
21. Yu, T. *et al.* Sub-MIC antibiotics increased the fitness cost of CRISPR-Cas in Acinetobacter baumannii. *Front Microbiol* **15**, 1381749 (2024).
22. Vale, P.F. *et al.* Costs of CRISPR-Cas-mediated resistance in Streptococcus thermophilus. *Proc Biol Sci* **282**, 20151270 (2015).

919 23. Westra, E.R. *et al.* Parasite Exposure Drives Selective Evolution of Constitutive versus
920 Inducible Defense. *Curr Biol* **25**, 1043-1049 (2015).
921 24. Meaden, S. *et al.* Correction: Phage gene expression and host responses lead to infection-
922 dependent costs of CRISPR immunity. *ISME J* **15**, 2491 (2021).
923 25. Zaayman, M. & Wheatley, R.M. Fitness costs of CRISPR-Cas systems in bacteria.
924 *Microbiology (Reading)* **168** (2022).
925 26. Chaudhry, W. *et al.* Mucoidy, a general mechanism for maintaining lytic phage in
926 populations of bacteria. *FEMS Microbiol Ecol* **96** (2020).
927 27. Wielgoss, S., Bergmiller, T., Bischofberger, A.M. & Hall, A.R. Adaptation to Parasites and
928 Costs of Parasite Resistance in Mutator and Nonmutator Bacteria. *Mol Biol Evol* **33**, 770-
929 782 (2016).
930 28. Scanlan, P.D. & Buckling, A. Co-evolution with lytic phage selects for the mucoid
931 phenotype of Pseudomonas fluorescens SBW25. *ISME J* **6**, 1148-1158 (2012).
932 29. MacGillivray, K.A. *et al.* Trade-offs constrain adaptive pathways to the type VI secretion
933 system survival. *iScience* **26**, 108332 (2023).
934 30. Gomez, P. & Buckling, A. Bacteria-phage antagonistic coevolution in soil. *Science* **332**, 106-
935 109 (2011).
936 31. York, D., Welch, K., Goryshin, I.Y. & Reznikoff, W.S. Simple and efficient generation in vitro
937 of nested deletions and inversions: Tn5 intramolecular transposition. *Nucleic Acids Res* **26**,
938 1927-1933 (1998).
939 32. Trotereau, J. *et al.* Construction and characterization of a saturated Tn-seq library of
940 Salmonella Typhimurium ATCC 14028. *Microbiol Resour Announc* **12**, e0036523 (2023).
941 33. Whichard, J.M. *et al.* Complete genomic sequence of bacteriophage felix o1. *Viruses* **2**,
942 710-730 (2010).
943 34. Vander Byl, C. & Kropinski, A.M. Sequence of the genome of Salmonella bacteriophage
944 P22. *J Bacteriol* **182**, 6472-6481 (2000).
945 35. Lee, J.H., Shin, H., Choi, Y. & Ryu, S. Complete genome sequence analysis of bacterial-
946 flagellum-targeting bacteriophage chi. *Arch Virol* **158**, 2179-2183 (2013).
947 36. Nguyen, Y. & Sperandio, V. Enterohemorrhagic E. coli (EHEC) pathogenesis. *Front Cell Infect*
948 *Microbiol* **2**, 90 (2012).
949 37. Davin-Regli, A. & Pages, J.M. Enterobacter aerogenes and Enterobacter cloacae; versatile
950 bacterial pathogens confronting antibiotic treatment. *Front Microbiol* **6**, 392 (2015).
951 38. Galan, J.E. Salmonella Typhimurium and inflammation: a pathogen-centric affair. *Nat Rev*
952 *Microbiol* **19**, 716-725 (2021).
953 39. Vis, M.A.M., Ito, K. & Hofmann, S. Impact of Culture Medium on Cellular Interactions in in
954 vitro Co-culture Systems. *Front Bioeng Biotechnol* **8**, 911 (2020).
955 40. Rostol, J.T. & Marraffini, L. (Ph)ighting Phages: How Bacteria Resist Their Parasites. *Cell*
956 *Host Microbe* **25**, 184-194 (2019).
957 41. Baxa, U. *et al.* Interactions of phage P22 tails with their cellular receptor, Salmonella O-
958 antigen polysaccharide. *Biophys J* **71**, 2040-2048 (1996).
959 42. Hudson, H.P., Lindberg, A.A. & Stocker, B.A. Lipopolysaccharide core defects in Salmonella
960 typhimurium mutants which are resistant to Felix O phage but retain smooth character. *J*
961 *Gen Microbiol* **109**, 97-112 (1978).

962 43. Nakao, R., Ramstedt, M., Wai, S.N. & Uhlin, B.E. Enhanced biofilm formation by Escherichia
963 coli LPS mutants defective in Hep biosynthesis. *PLoS One* **7**, e51241 (2012).
964 44. Ge, H. *et al.* The rfbN gene of Salmonella Typhimurium mediates phage adsorption by
965 modulating biosynthesis of lipopolysaccharide. *Microbiol Res* **250**, 126803 (2021).
966 45. Beck, C.M. *et al.* CdiA from Enterobacter cloacae delivers a toxic ribosomal RNase into
967 target bacteria. *Structure* **22**, 707-718 (2014).
968 46. Whitney, J.C. *et al.* Genetically distinct pathways guide effector export through the type VI
969 secretion system. *Mol Microbiol* **92**, 529-542 (2014).
970 47. Hood, R.D. *et al.* A type VI secretion system of Pseudomonas aeruginosa targets a toxin to
971 bacteria. *Cell Host Microbe* **7**, 25-37 (2010).
972 48. Aoki, S.K. *et al.* Contact-dependent inhibition of growth in Escherichia coli. *Science* **309**,
973 1245-1248 (2005).
974 49. Hersch, S.J., Manera, K. & Dong, T.G. Defending against the Type Six Secretion System:
975 beyond Immunity Genes. *Cell Rep* **33**, 108259 (2020).
976 50. Toska, J., Ho, B.T. & Mekalanos, J.J. Exopolysaccharide protects Vibrio cholerae from
977 exogenous attacks by the type 6 secretion system. *Proc Natl Acad Sci U S A* **115**, 7997-
978 8002 (2018).
979 51. Flaugnatti, N. *et al.* Human commensal gut Proteobacteria withstand type VI secretion
980 attacks through immunity protein-independent mechanisms. *Nat Commun* **12**, 5751
981 (2021).
982 52. West, N.P. *et al.* Optimization of virulence functions through glucosylation of Shigella LPS.
983 *Science* **307**, 1313-1317 (2005).
984 53. Papo, N. & Shai, Y. A molecular mechanism for lipopolysaccharide protection of Gram-
985 negative bacteria from antimicrobial peptides. *J Biol Chem* **280**, 10378-10387 (2005).
986 54. Bertani, B. & Ruiz, N. Function and Biogenesis of Lipopolysaccharides. *EcoSal Plus* **8** (2018).
987 55. Kaniuk, N.A., Vinogradov, E. & Whitfield, C. Investigation of the structural requirements in
988 the lipopolysaccharide core acceptor for ligation of O antigens in the genus Salmonella:
989 WaaL "ligase" is not the sole determinant of acceptor specificity. *J Biol Chem* **279**, 36470-
990 36480 (2004).
991 56. Di Lorenzo, F. *et al.* A Journey from Structure to Function of Bacterial Lipopolysaccharides.
992 *Chem Rev* **122**, 15767-15821 (2022).
993 57. Bastin, D.A., Stevenson, G., Brown, P.K., Haase, A. & Reeves, P.R. Repeat unit
994 polysaccharides of bacteria: a model for polymerization resembling that of ribosomes and
995 fatty acid synthetase, with a novel mechanism for determining chain length. *Mol Microbiol*
996 **7**, 725-734 (1993).
997 58. Murray, G.L., Attridge, S.R. & Morona, R. Regulation of Salmonella typhimurium
998 lipopolysaccharide O antigen chain length is required for virulence; identification of FepE
999 as a second Wzz. *Mol Microbiol* **47**, 1395-1406 (2003).
1000 59. Murray, G.L., Attridge, S.R. & Morona, R. Altering the length of the lipopolysaccharide O
1001 antigen has an impact on the interaction of Salmonella enterica serovar Typhimurium with
1002 macrophages and complement. *J Bacteriol* **188**, 2735-2739 (2006).
1003 60. Zhang, G., Meredith, T.C. & Kahne, D. On the essentiality of lipopolysaccharide to Gram-
1004 negative bacteria. *Curr Opin Microbiol* **16**, 779-785 (2013).

1005 61. Schwarz, S. *et al.* Burkholderia type VI secretion systems have distinct roles in eukaryotic
1006 and bacterial cell interactions. *PLoS Pathog* **6**, e1001068 (2010).
1007 62. Simpson, B.W. & Trent, M.S. Pushing the envelope: LPS modifications and their
1008 consequences. *Nat Rev Microbiol* **17**, 403-416 (2019).
1009 63. Steinbacher, S. *et al.* Phage P22 tailspike protein: crystal structure of the head-binding
1010 domain at 2.3 A, fully refined structure of the endorhamnosidase at 1.56 A resolution, and
1011 the molecular basis of O-antigen recognition and cleavage. *J Mol Biol* **267**, 865-880 (1997).
1012 64. Eriksson, U., Svenson, S.B., Lonngren, J. & Lindberg, A.A. Salmonella phage glycanases:
1013 substrate specificity of the phage P22 endo-rhamnosidase. *J Gen Virol* **43**, 503-511 (1979).
1014 65. Steinbacher, S. *et al.* Crystal structure of P22 tailspike protein: interdigitated subunits in a
1015 thermostable trimer. *Science* **265**, 383-386 (1994).
1016 66. Waseh, S. *et al.* Orally administered P22 phage tailspike protein reduces salmonella
1017 colonization in chickens: prospects of a novel therapy against bacterial infections. *PLoS*
1018 *One* **5**, e13904 (2010).
1019 67. Tang, J. *et al.* Peering down the barrel of a bacteriophage portal: the genome packaging
1020 and release valve in p22. *Structure* **19**, 496-502 (2011).
1021 68. Sonani, R.R., Esteves, N.C., Scharf, B.E. & Egelman, E.H. Cryo-EM structure of flagellotropic
1022 bacteriophage Chi. *Structure* **32**, 856-865 e853 (2024).
1023 69. Snyder, D.S. & McIntosh, T.J. The lipopolysaccharide barrier: correlation of antibiotic
1024 susceptibility with antibiotic permeability and fluorescent probe binding kinetics.
1025 *Biochemistry* **39**, 11777-11787 (2000).
1026 70. Delcour, A.H. Outer membrane permeability and antibiotic resistance. *Biochim Biophys*
1027 *Acta* **1794**, 808-816 (2009).
1028 71. Zgurskaya, H.I., Lopez, C.A. & Gnanakaran, S. Permeability Barrier of Gram-Negative Cell
1029 Envelopes and Approaches To Bypass It. *ACS Infect Dis* **1**, 512-522 (2015).
1030 72. Vaara, M. Agents that increase the permeability of the outer membrane. *Microbiol Rev* **56**,
1031 395-411 (1992).
1032 73. Helander, I.M. & Mattila-Sandholm, T. Fluorometric assessment of gram-negative bacterial
1033 permeabilization. *J Appl Microbiol* **88**, 213-219 (2000).
1034 74. Bolla, J.M. *et al.* Strategies for bypassing the membrane barrier in multidrug resistant
1035 Gram-negative bacteria. *FEBS Lett* **585**, 1682-1690 (2011).
1036 75. Wang, Z., Wang, J., Ren, G., Li, Y. & Wang, X. Influence of Core Oligosaccharide of
1037 Lipopolysaccharide to Outer Membrane Behavior of Escherichia coli. *Mar Drugs* **13**, 3325-
1038 3339 (2015).
1039 76. Allsopp, L.P. & Bernal, P. Killing in the name of: T6SS structure and effector diversity.
1040 *Microbiology (Reading)* **169** (2023).
1041 77. Dufrene, Y.F. Atomic force microscopy, a powerful tool in microbiology. *J Bacteriol* **184**,
1042 5205-5213 (2002).
1043 78. Strauss, J., Burnham, N.A. & Camesano, T.A. Atomic force microscopy study of the role of
1044 LPS O-antigen on adhesion of E. coli. *J Mol Recognit* **22**, 347-355 (2009).
1045 79. Kahli, H. *et al.* Impact of Growth Conditions on Pseudomonas fluorescens Morphology
1046 Characterized by Atomic Force Microscopy. *Int J Mol Sci* **23** (2022).
1047 80. Pagnout, C. *et al.* Pleiotropic effects of rfa-gene mutations on Escherichia coli envelope
1048 properties. *Sci Rep* **9**, 9696 (2019).

1049 81. Souza, D.P. *et al.* Bacterial killing via a type IV secretion system. *Nat Commun* **6**, 6453
1050 (2015).
1051 82. Bayer-Santos, E. *et al.* The opportunistic pathogen Stenotrophomonas maltophilia utilizes
1052 a type IV secretion system for interbacterial killing. *PLoS Pathog* **15**, e1007651 (2019).
1053 83. Sgro, G.G. *et al.* Bacteria-Killing Type IV Secretion Systems. *Front Microbiol* **10**, 1078 (2019).
1054 84. Wang, H., Liu, Y., Bai, C. & Leung, S.S.Y. [Not Available]. *Acta Pharm Sin B* **14**, 155-169
1055 (2024).
1056 85. Knecht, L.E., Veljkovic, M. & Fieseler, L. Diversity and Function of Phage Encoded
1057 Depolymerases. *Front Microbiol* **10**, 2949 (2019).
1058 86. Edwards, R.A., Keller, L.H. & Schifferli, D.M. Improved allelic exchange vectors and their
1059 use to analyze 987P fimbria gene expression. *Gene* **207**, 149-157 (1998).
1060 87. Gibson, D.G. *et al.* Enzymatic assembly of DNA molecules up to several hundred kilobases.
1061 *Nat Methods* **6**, 343-345 (2009).
1062 88. Kunkel, T.A. Rapid and efficient site-specific mutagenesis without phenotypic selection.
1063 *Proc Natl Acad Sci U S A* **82**, 488-492 (1985).
1064 89. Lee, P.C., Stopford, C.M., Svenson, A.G. & Rietsch, A. Control of effector export by the
1065 Pseudomonas aeruginosa type III secretion proteins PcrG and PcrV. *Mol Microbiol* **75**, 924-
1066 941 (2010).
1067 90. McKenzie, G.J. & Craig, N.L. Fast, easy and efficient: site-specific insertion of transgenes
1068 into enterobacterial chromosomes using Tn7 without need for selection of the insertion
1069 event. *BMC Microbiol* **6**, 39 (2006).
1070 91. Mandal, R.K., Jiang, T. & Kwon, Y.M. Genetic Determinants in Salmonella enterica Serotype
1071 Typhimurium Required for Overcoming In Vitro Stressors in the Mimicking Host
1072 Environment. *Microbiol Spectr* **9**, e0015521 (2021).
1073 92. Liu, Q. *et al.* Immunogenicity and Cross-Protective Efficacy Induced by Outer Membrane
1074 Proteins from Salmonella Typhimurium Mutants with Truncated LPS in Mice. *Int J Mol Sci*
1075 **17**, 416 (2016).
1076 93. Chen, P.Y. *et al.* A whole-cell platform for discovering synthetic cell adhesion molecules in
1077 bacteria. *Nat Commun* **15**, 6568 (2024).
1078 94. Ting, S.Y. *et al.* Targeted Depletion of Bacteria from Mixed Populations by Programmable
1079 Adhesion with Antagonistic Competitor Cells. *Cell Host Microbe* **28**, 313-321 e316 (2020).
1080 95. Miller, S., Schuler, B. & Seckler, R. Phage P22 tailspike protein: removal of head-binding
1081 domain unmasks effects of folding mutations on native-state thermal stability. *Protein Sci*
1082 **7**, 2223-2232 (1998).
1083 96. Muheim, C. *et al.* Increasing the permeability of Escherichia coli using MAC13243. *Sci Rep*
1084 **7**, 17629 (2017).
1085 97. Oh, Y.J. Use of Atomic Force Microscopy to Characterize LPS Perturbations. *Methods Mol*
1086 *Biol* **2548**, 279-287 (2022).
1087 98. Singh, S. *et al.* LPS O Antigen Plays a Key Role in Klebsiella pneumoniae Capsule Retention.
1088 *Microbiol Spectr* **10**, e0151721 (2022).
1089 99. Gavara, N. A beginner's guide to atomic force microscopy probing for cell mechanics.
1090 *Microsc Res Tech* **80**, 75-84 (2017).
1091 100. Steinbacher, S. *et al.* Crystal structure of phage P22 tailspike protein complexed with
1092 Salmonella sp. O-antigen receptors. *Proc Natl Acad Sci U S A* **93**, 10584-10588 (1996).

1093 **Supplementary Table 1. Strains, Recombinant DNA, and Oligonucleotides used in this**
1094 **study.**
1095

Strain	**Source**	**Identifier**
Escherichia coli DH5α	YB Biotech	Cat# XR-LYE678-80
Escherichia coli PIR1	Gift from Dr. Hsin-Hung David Chou	N/A
Escherichia coli BL21 pRIL (DE3)	Gift from Dr. Hung-Ta Chen	N/A
Escherichia coli S17-1 λ pir	Lab collection	N/A
Enterobacter cloacae	American Type Culture Collection	ATCC 13047
Enterobacter cloacae Δ*tssM*	Whitney *et al.*, 2014	N/A
Enterobacter cloacae Δ*cdiA*	Beck *et al.*, 2015	N/A
Salmonella enterica serovar Typhimurium	American Type Culture Collection	ATCC 14028
Salmonella enterica serovar Typhimurium Tn7::Chl	This paper	N/A
Salmonella enterica serovar Typhimurium LT2/(P22)+	Bioresource Collection and Research Center	BCRC 12459
Salmonella enterica bacteriophage Felix O1	Leibniz Institute DSMZ	DSM 18524
Salmonella enterica bacteriophage Chi	American Type Culture Collection	ATCC 9842-B1
Salmonella enterica bacteriophage As1	This paper	N/A
Salmonella enterica bacteriophage As2	This paper	N/A
Salmonella enterica bacteriophage As3	This paper	N/A
Salmonella enterica bacteriophage As4	This paper	N/A
Salmonella enterica serovar Typhimurium Tn7::Chl Δ*waaL*	This paper	N/A
Salmonella enterica serovar Typhimurium Tn7::Chl Δ*waaJ*	This paper	N/A
Salmonella enterica serovar Typhimurium Tn7::Chl Δ*waaO*	This paper	N/A
Salmonella enterica serovar Typhimurium Tn7::Chl Δ*waaG*	This paper	N/A
Salmonella enterica serovar Typhimurium Tn7::Chl Δ*waaK*	This paper	N/A
Salmonella enterica serovar Typhimurium Tn7::Chl Δ*waaB*	This paper	N/A
Salmonella enterica serovar Typhimurium Tn7::Chl Δ*waaQ*	This paper	N/A

Salmonella enterica serovar Typhimurium Tn7::Chl Δ*waaY*	This paper	N/A
Salmonella enterica serovar Typhimurium Tn7::Chl Δ*wzzB*	This paper	N/A
Salmonella enterica serovar Typhimurium Tn7::Chl Δ*fepE*	This paper	N/A
Enterohemorrhagic *Escherichia coli* O157:H7 EDL933	American Type Culture Collection	ATCC-43895
Enterohemorrhagic *Escherichia coli* O157:H7 EDL933 Tn7::Chl	This paper	N/A
Enterohemorrhagic *Escherichia coli* O157:H7 EDL933 Tn7::Chl Δ*waaO*	This paper	N/A
Citrobacter rodentium DBS100	American Type Culture Collection	ATCC-51459
Citrobacter rodentium DBS100 Δ*waaO*	This paper	N/A
Burkholderia thailandensis E264	American Type Culture Collection	ATCC-700388
Burkholderia thailandensis E264 Δ*tssM*	LeRoux *et al.*, 2015	N/A
Felix O1-resistant *Salmonella enterica* serovar Typhimurium-R1	This paper	N/A
Felix O1-resistant *Salmonella enterica* serovar Typhimurium-R2	This paper	N/A
Felix O1-resistant *Salmonella enterica* serovar Typhimurium-R3	This paper	N/A
Felix O1-resistant *Salmonella enterica* serovar Typhimurium-R4	This paper	N/A
Felix O1-resistant *Salmonella enterica* serovar Typhimurium-R5	This paper	N/A
Felix O1-resistant *Salmonella enterica* serovar Typhimurium-R6	This paper	N/A
Felix O1-resistant *Salmonella enterica* serovar Typhimurium-R7	This paper	N/A
Felix O1-resistant *Salmonella enterica* serovar Typhimurium-R8	This paper	N/A
Felix O1-resistant *Salmonella enterica* serovar Typhimurium-R9	This paper	N/A
P22-resistant *Salmonella enterica* serovar Typhimurium-R1	This paper	N/A
P22-resistant *Salmonella enterica* serovar Typhimurium-R2	This paper	N/A
P22-resistant *Salmonella enterica* serovar Typhimurium-R3	This paper	N/A

P22-resistant *Salmonella enterica* serovar Typhimurium-R4	This paper	N/A
P22-resistant *Salmonella enterica* serovar Typhimurium-R5	This paper	N/A
P22-resistant *Salmonella enterica* serovar Typhimurium-R6	This paper	N/A
P22-resistant *Salmonella enterica* serovar Typhimurium-R7	This paper	N/A
P22-resistant *Salmonella enterica* serovar Typhimurium-R8	This paper	N/A
P22-resistant *Salmonella enterica* serovar Typhimurium-R9	This paper	N/A
Chi-resistant *Salmonella enterica* serovar Typhimurium-R1	This paper	N/A
Chi-resistant *Salmonella enterica* serovar Typhimurium-R2	This paper	N/A
Chi-resistant *Salmonella enterica* serovar Typhimurium-R3	This paper	N/A
Chi-resistant *Salmonella enterica* serovar Typhimurium-R4	This paper	N/A
Chi-resistant *Salmonella enterica* serovar Typhimurium-R5	This paper	N/A
Chi-resistant *Salmonella enterica* serovar Typhimurium-R6	This paper	N/A
Chi-resistant *Salmonella enterica* serovar Typhimurium-R7	This paper	N/A
Chi-resistant *Salmonella enterica* serovar Typhimurium-R8	This paper	N/A
Chi-resistant *Salmonella enterica* serovar Typhimurium-R9	This paper	N/A

1096

Recombinant DNA	**Source**
pRE118_SentΔ*waaL*	This paper
pRE118_SentΔ*waaJ*	This paper
pRE118_SentΔ*waaO*	This paper
pRE118_SentΔ*waaG*	This paper
pRE118_SentΔ*waaK*	This paper
pRE118_SentΔ*waaB*	This paper
pRE118_SentΔ*waaQ*	This paper
pRE118_SentΔ*waaY*	This paper
pRE118_SentΔ*wzzB*	This paper
pRE118_SentΔ*fepE*	This paper
pPSV39_SentWzzB	This paper
pPSV39_SentFepE	This paper
pRE118_EcoliΔ*waaO*	This paper

pRE118_CrodΔ*waaO*	This paper
pETDuet-1-His6_P22TSP	This paper
pETDuet-1-His6_P22TSP D392N	This paper
pGRG37	McKenzie *et al.* 2006

1097

Primer	**Sequences (5'-3')**	**Identifier**
Bacteria strain construction		
Sent_ΔwaaL_F1	CATGAATTCCCGGGAGAGCTCATCAAAGCGGAACGCACAG	Mission Biotech
Sent_ΔwaaL_R1	TTTATCTATTGGTTAGCATCTTTTCTCCACAATAG	Mission Biotech
Sent_ΔwaaL_F2	GATGCTAACCAATAGATAAAAAAACGCGC	Mission Biotech
Sent_ΔwaaL_R2	CGACGGATCCCAAGCTTCTTCTAGAACCAGAACTTCCTGATAATG	Mission Biotech
Sent_ΔwaaL_seq_F	TGATTCCCGTCGCTATTCGC	Mission Biotech
Sent_ΔwaaL_seq_R	AGATCAGAGAGCGCAATCCG	Mission Biotech
Sent_ΔwaaJ_F1	CATGAATTCCCGGGAGAGCTCGTACGCTACGCAGATTGTTG	Mission Biotech
Sent_ΔwaaJ_R1	ATTATTTGTGTGAATCCATTACATCACCTATG	Mission Biotech
Sent_ΔwaaJ_F2	AATGGATTCACACAAATAATTCCCCTCC	Mission Biotech
Sent_ΔwaaJ_R2	CGACGGATCCCAAGCTTCTTCTAGACCTTACCCTTAATACGAC	Mission Biotech
Sent_ΔwaaJ_seq_F	TGAAGACCAGCAGCGATTTG	Mission Biotech
Sent_ΔwaaJ_seq_R	ACGTGCTACATTGATCAGCG	Mission Biotech
Sent_ΔwaaO_F1	CATGAATTCCCGGGAGAGCTCGTGATATGTATTGATGTCATCTC	Mission Biotech
Sent_ΔwaaO_R1	TTTATTCAAGTCTGCTCATAGTGATCAC	Mission Biotech
Sent_ΔwaaO_F2	TATGAGCAGACTTGAATAAAACCCATAGGTG	Mission Biotech
Sent_ΔwaaO_R2	CGACGGATCCCAAGCTTCTTCTAGAGTGACTTATCTTTCAACTCAC	Mission Biotech
Sent_ΔwaaO_seq_F	CTTCGTCGAGCTAAGCATG	Mission Biotech
Sent_ΔwaaO_seq_R	TGTAGCGCCCGTATAATG	Mission Biotech
Sent_ΔwaaG_F1	CATGAATTCCCGGGAGAGCTCAATCTCACCGATCAGTGG	Mission Biotech
Sent_ΔwaaG_R1	CTCAACCATCAACTCTCATAGCAGGCTG	Mission Biotech

Sent_ΔwaaG_F2	TATGAGAGTTGATGGTTGAGCTGAAAGC	Mission Biotech
Sent_ΔwaaG_R2	CGACGGATCCCAAGCTTCTTCTAGACACTCATAAATTACTCACTGAG	Mission Biotech
Sent_ΔwaaG_seq_F	AGATCAAAAACGCGCTATCG	Mission Biotech
Sent_ΔwaaG_seq_R	GCAATGTCCAGTCTTCTTCC	Mission Biotech
Sent_ΔwaaK_F1	CATGAATTCCCGGGAGAGCTCAAGATGTCATTGCAGTCAATG	Mission Biotech
Sent_ΔwaaK_R1	ATCACTTATCTTTAATCATAATAGCTATAATCCAGAATAG	Mission Biotech
Sent_ΔwaaK_F2	TATGATTAAAGATAAGTGATTGAGTCCTG	Mission Biotech
Sent_ΔwaaK_R2	CGACGGATCCCAAGCTTCTTCTAGACATCGACATATGTCCGATTC	Mission Biotech
Sent_ΔwaaK_seq_F	GGTCCTACGTCCAGAAAGAC	Mission Biotech
Sent_ΔwaaK_seq_R	TTTAGGACTTCGCTGCCTTG	Mission Biotech
Sent_ΔwaaB_F1	CATGAATTCCCGGGAGAGCTCGAAGACTACTGTGCTGAC	Mission Biotech
Sent_ΔwaaB_R1	ATCACTTTTGTATTTTCATATATACCCCAGAG	Mission Biotech
Sent_ΔwaaB_F2	TATGAAAATACAAAAGTGATCACTATGAGC	Mission Biotech
Sent_ΔwaaB_R2	CGACGGATCCCAAGCTTCTTCTAGATACAGTCTCAGCATCAAC	Mission Biotech
Sent_ΔwaaB_seq_F	TGGGCGTTGATACGATGCAC	Mission Biotech
Sent_ΔwaaB_seq_R	ACTATGCCAGGGCTTCGTTG	Mission Biotech
Sent_ΔwaaQ_F1	CATGAATTCCCGGGAGAGCTCGTGCAGCGCAGCAATCAG	Mission Biotech
Sent_ΔwaaQ_R1	CTCATAGCAGCTTTTCCACAAGCGACTCTTTG	Mission Biotech
Sent_ΔwaaQ_F2	TGTGGAAAAGCTGCTATGAGAGTTGCCTTTTG	Mission Biotech
Sent_ΔwaaQ_R2	CGACGGATCCCAAGCTTCTTCTAGACCATTAACTCCGCGATATC	Mission Biotech
Sent_ΔwaaQ_seq_F	GCGCATTAGCGATAACCAGG	Mission Biotech
Sent_ΔwaaQ_seq_R	CCTGATAGGCTGGATGCAG	Mission Biotech
Sent_ΔwaaY_F1	for making Salmonella 14028 ChlR waaY/rfaY (EJJ31_RS00655) deletion with pRE118	Mission Biotech
Sent_ΔwaaY_R1	ATCAGCGTTTAATAATCATAATGGAGATTTAGGG	Mission Biotech

Sent_ΔwaaY_F2	TATGATTATTAAACGCTGATCAATGTAG	Mission Biotech
Sent_ΔwaaY_R2	CGACGGATCCCAAGCTTCTTCTAGAATTCGTCATAGAAACGTG	Mission Biotech
Sent_ΔwaaY_seq_F	GTTTAGCCGTACAGCATCAC	Mission Biotech
Sent_ΔwaaY_seq_R	TAAGCTCAGATGGCATAGGG	Mission Biotech
Sent_ΔwzzB_F1	CATGAATTCCCGGGAGAGCTCACTCCAGGAAGGCGCTATTAAAC	Mission Biotech
Sent_ΔwzzB_R1	CTTACAAGGCCACTGTCATAGATACCCTAACTAAAAAAAGGATG	Mission Biotech
Sent_ΔwzzB_F2	TATGACAGTGGCCTTGTAAGCTTCTTTGCCGGATG	Mission Biotech
Sent_ΔwzzB_R2	CGACGGATCCCAAGCTTCTTCTAGATGTCGACGGCGCGC	Mission Biotech
Sent_ΔwzzB_seq_F	CGTGATTGGGGAACAGTCTG	Mission Biotech
Sent_ΔwzzB_seq_R	CTTGAGGCATTCCGTGATGC	Mission Biotech
Sent_ΔfepE_F1	CATGAATTCCCGGGAGAGCTCCTATACCGTCGCAAAAAACC	Mission Biotech
Sent_ΔfepE_R1	CATGCCATCTTTAGTCTGATTTACCCGAAAAGC	Mission Biotech
Sent_ΔfepE_F2	ATCAGACTAAAGATGGCATGCCGTATGAC	Mission Biotech
Sent_ΔfepE_R2	CGACGGATCCCAAGCTTCTTCTAGAAGGTATGTGAACATCATC	Mission Biotech
Sent_ΔfepE_seq_F	CCTATGCAAACCGCAACCACCC	Mission Biotech
Sent_ΔfepE_seq_R	CCGAATCCGTAGCCCGTTTGC	Mission Biotech
Sent_WzzB_F	ACAATTTCAGAATTCGAGCTCATGACAGTGGATAGTAATACGTC	Mission Biotech
Sent_WzzB_R	TCATTTCAATATCTGTATATCTAGATTACAAGGCTTTTGGCTTATAGC	Mission Biotech
Sent_FepE_F	ACAATTTCAGAATTCGAGCTCATGCCATCTCTTAATGTAAAACAAG	Mission Biotech
Sent_FepE_R	TCATTTCAATATCTGTATATCTAGATCAGACTAACCGTTCATCTATC	Mission Biotech
Ecoli_ΔwaaO_F1	CATGAATTCCCGGGAGAGCTCCGTTATGGCGCGGTAAAG	Mission Biotech

Ecoli_ΔwaaO_R1	TTTAGAAGCATTGAGACATATTTATTCTGTATCCAAAATTTTG	Mission Biotech
Ecoli_ΔwaaO_F2	TATGTCTCAATGCTTCTAAAGATTTAAGGTTAAAATAATTC	Mission Biotech
Ecoli_ΔwaaO_R2	CGACGGATCCCAAGCTTCTTCTAGAGCGCTTGTCCAGTTCAATTATATC	Mission Biotech
Ecoli_ΔwaaO_seq_F	GATGGTTGAACTTAAAGAGCCG	Mission Biotech
Ecoli_ΔwaaO_seq_R	CCTGGTAGTTCTCATCAATACC	Mission Biotech
Crod_ΔwaaO_F1	CATGAATTCCCGGGAGAGCTCCGTTATGGCGCGGTAAAG	Mission Biotech
Crod_ΔwaaO_R1	TTTAGAAGCATTGAGACATATTTATTCTGTATCCAAAATTTTG	Mission Biotech
Crod_ΔwaaO_F2	TATGTCTCAATGCTTCTAAAGATTTAAGGTTAAAATAATTC	Mission Biotech
Crod_ΔwaaO_R2	CGACGGATCCCAAGCTTCTTCTAGAGCGCTTGTCCAGTTCAATTATATC	Mission Biotech
Crod_ΔwaaO_seq_F	ATTAATGCATTTAGCCAGTGGC	Mission Biotech
Crod_ΔwaaO_seq_R	TGTATCTTCTGAAATTATGCGC	Mission Biotech
Plasmid construction		
pETDuet_TSP_F	ACCATCATCACCACAGCCAGGATCCAGATCAATATTCAATAGAAGC	Mission Biotech
pETDuet_TSP_R	GTTCGACTTAAGCATTATGCGGCCGCTAAAGTGTTGCCAAGGTTAATCTAACTAATTC	Mission Biotech
pETDuet_TSP_D392N_F	CCCCGTATGGAATGGATTCGATTTAGGTGCTGAC	Mission Biotech
pETDuet_TSP_D392N_R	CGAATCCATTCCATACGGGGTAAATAACGACC	Mission Biotech
pETDuet_Seq_F	ATGCGTCCGGCGTAGA	Mission Biotech
pETDuet_Seq_R	GATTATGCGGCCGTGTACAA	Mission Biotech
pRE118_seq_F	GGTTGAGAAGCGGTGTAAGTG	Mission Biotech
pRE118_seq_R	GCAGGTCGATCCCAAGCTTC	Mission Biotech
pPSV39_seq_F	GGATTACGTGGCCTGTAGAC	Mission Biotech
pPSV39_seq_R	CCCGTTTAGAGGCCCC	Mission Biotech
Transposon Insertion mapping		

EzTn5_s	GATCCTCTAGAGTCGACCTGCAGGCATGCA	Integrated DNA Technologies, Inc.
Tn5_F	TCGTCGGCAGCGTCAGATGTGTATAAGAGACAG	Integrated DNA Technologies, Inc.
Tn5_R	GTCTCGTGGGCTCGGAGATGTGTATAAGAGACAGGGGGGGGGGGGGGGG	Integrated DNA Technologies, Inc.

1100

Figure 1

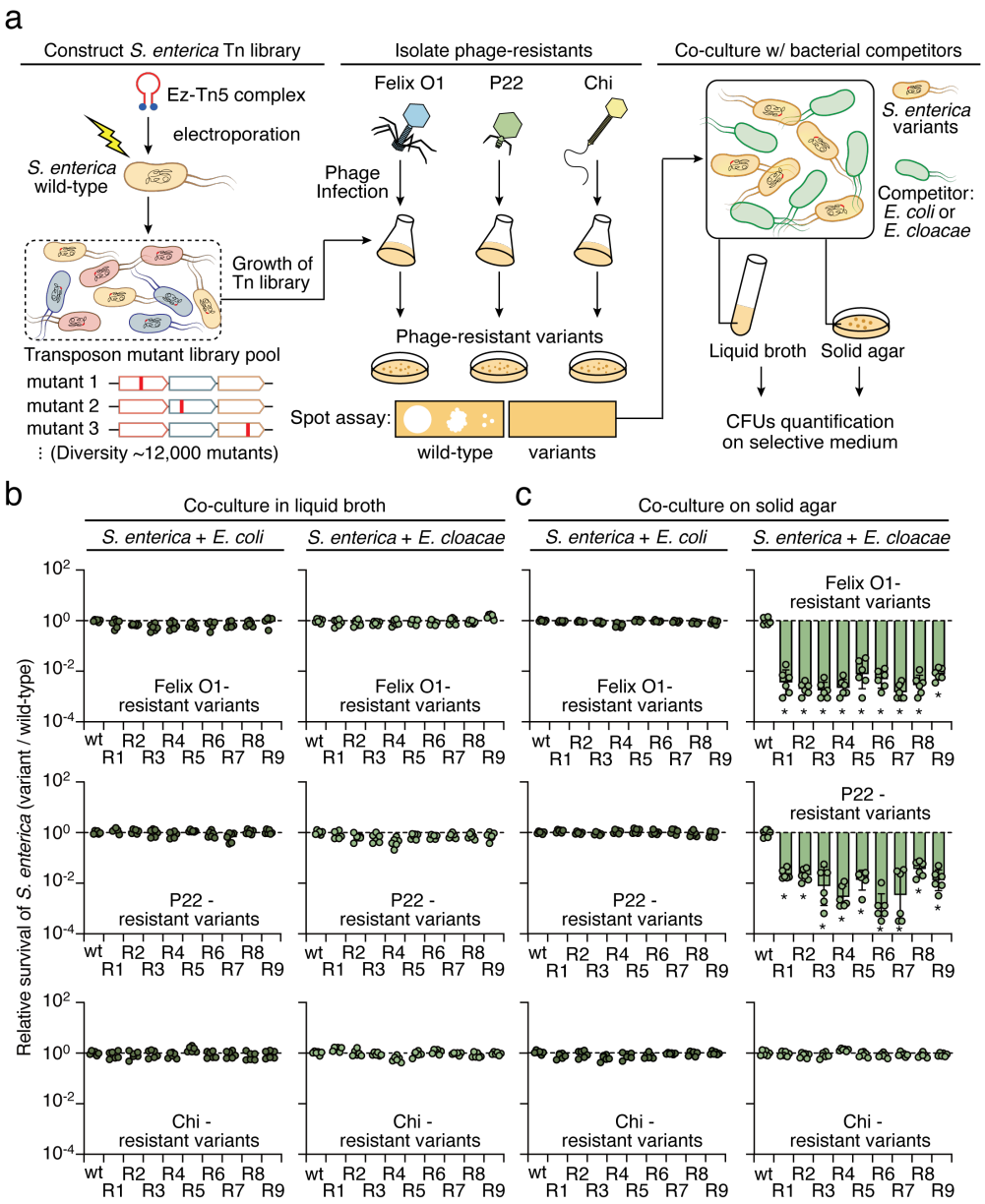

Figure 1. Isolation of phage-resistant *S. enterica* for pairwise co-culture experiments. (a) Schematic workflow for isolating phage-resistant strains from a transposon library (Tn-library) pool containing approximately 12,000 mutants. Detailed procedures are provided in the Methods section. Phages from different families of Caudovirales were used for selection: Felix O1, P22, and Chi (**Supplementary Figure 1a**). Spot assays were employed to validate the resistance of the isolated strains to phage infections (**Supplementary Figure 1b**). Validated resistant variants were subsequently co-cultured with *E. coli* or *E. cloacae* in liquid broth or on solid agar. The survival of *S. enterica* was quantified by counting CFUs on selective media. (b, c) Relative survival of the indicated *S. enterica* strains compared to wild-type *S. enterica* grown in co-culture with *E. coli* or *E. cloacae* in LB broth (b) or solid agar (c). Relative survival was determined by comparing CFU ratios of phage-resistant variants and the wild-type control. Data in (b) and (c) are represented as means ± SD (n=6). Asterisks indicate statistically significant differences between the survival of a mutant strain and the wild-type control ($p < 0.05$).

1101

Figure 2

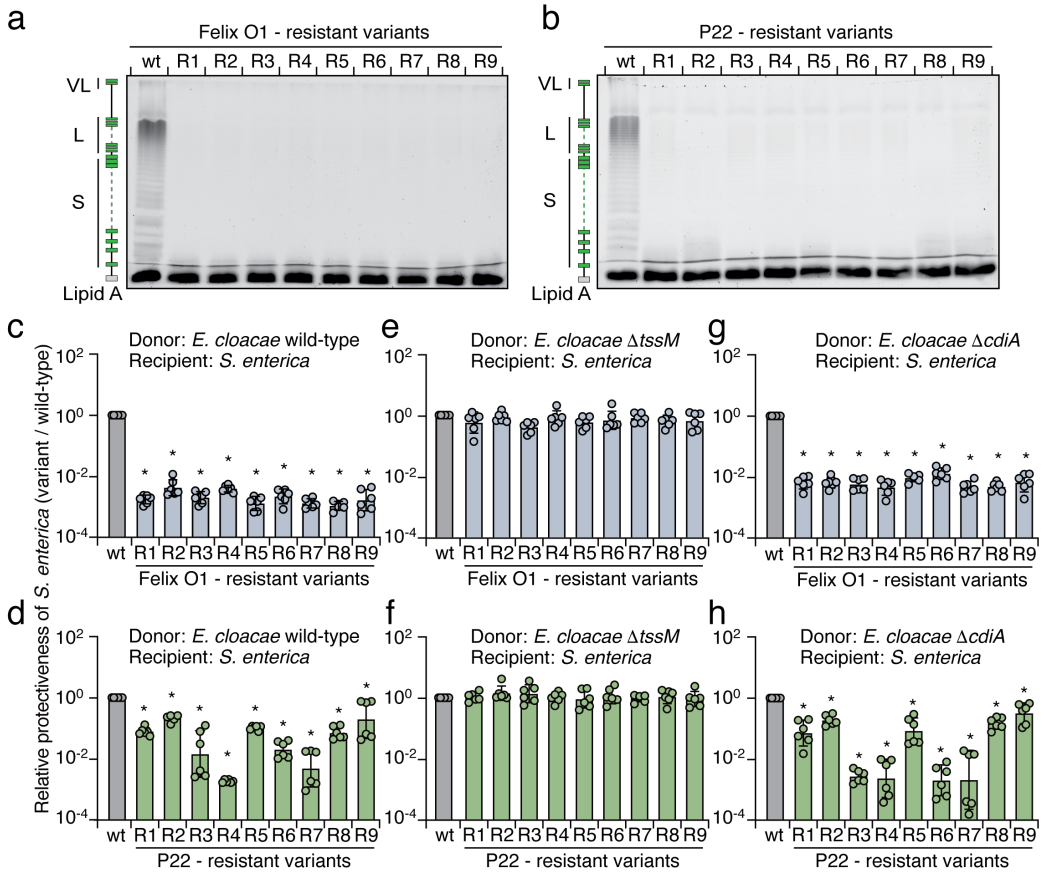

Figure 2. Phage-resistant strains exhibit LPS deficiency and increased susceptibility to T6SS-mediated antagonism by *E. cloacae*. (a, b) 12% LPS PAGE profiles showing the levels of LPS produced by the indicated *S. enterica* strains: (a) LPS from the Felix O1-resistant strains; (b) LPS from the P22-resistant strains. A schematic representation of LPS is shown on the left. (c-h) Protectiveness of the indicated *S. enterica* phage-resistant strains relative to the wild-type strain after competition with *E. cloacae* wild-type (c, d), Δ*tssM* (e, f), and Δ*cdiA* (g, h) strains. Data in (c-h) are presented as means ± SD (n=6). Asterisks indicate statistically significant differences between the relative protective index of a mutant strain and the wild-type control ($p < 0.05$).

1102

Figure 3

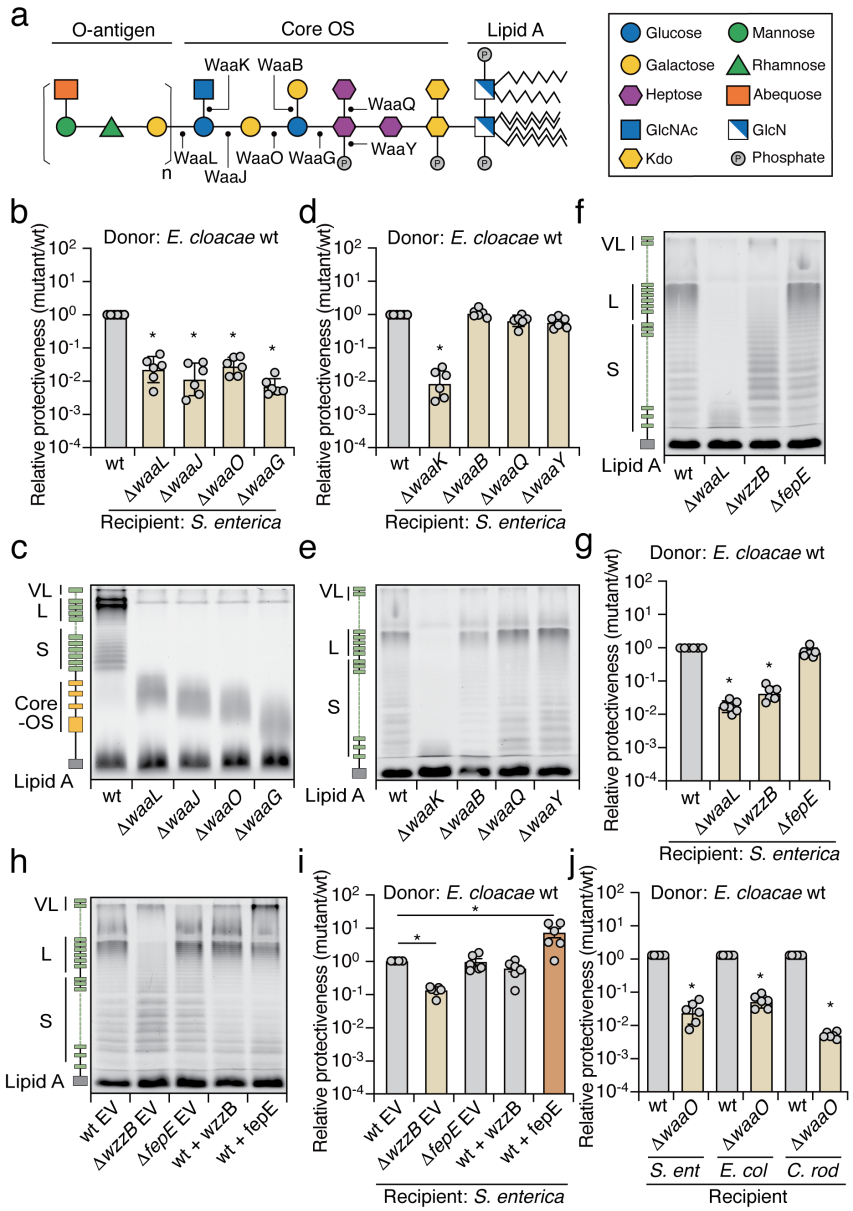

Figure 3. LPS protects bacteria from T6SS-mediated assaults. (a) Schematic representation of the LPS structure in *S. enterica*. Glycosyltransferases involved in LPS biosynthesis are indicated. (b, d, g, i) Protectiveness of the indicated *S. enterica* mutant or indicated protein overexpressing strains relative to the wild-type strain after competition with wild-type *E. cloacae*. (c, e, f, h) LPS PAGE profiles: (c) 20% gel; (e, f, h) 12% gel, showing LPS levels produced by the indicated *S. enterica* mutant or indicated protein overexpressing strains. EV, empty vector. (j) Protectiveness of the indicated bacterial species (Δ*waaO* mutant) relative to the wild-type strain after competition with wild-type *E. cloacae*. Data in (b, d, g, i, j) are presented as means ± SD (n=6). Asterisks indicate statistically significant differences between the relative protective index of a mutant strain and the wild-type control ($p < 0.05$).

1103

Figure 4

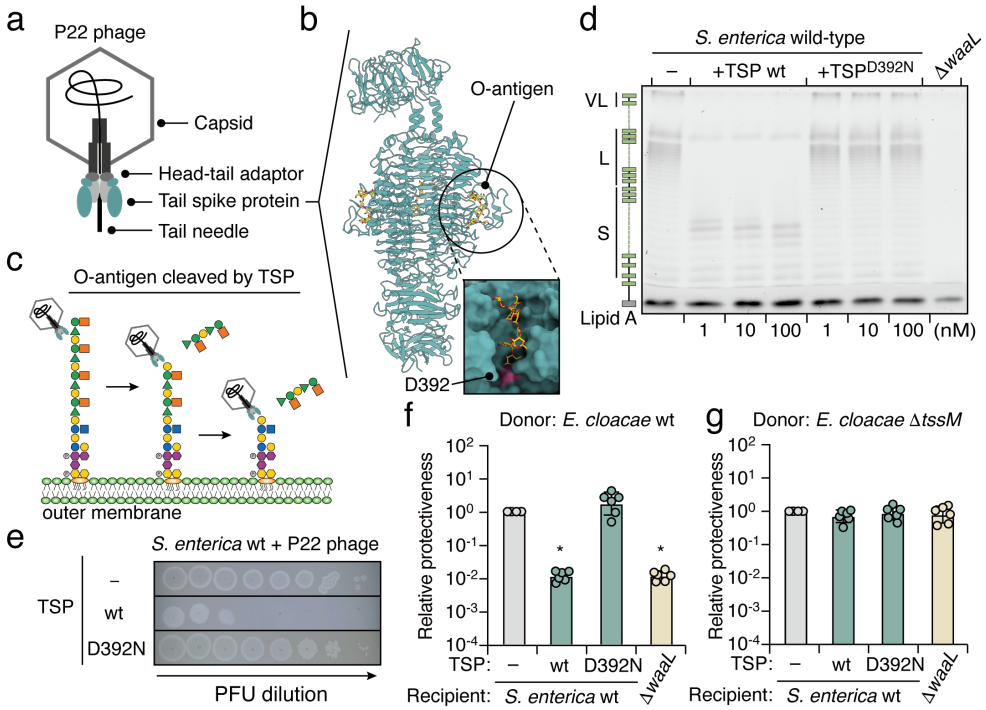

Figure 4. Purified TSP increases the susceptibility of *S. enterica* to T6SS-mediated intoxication. (a) Schematic illustration of phage P22. (b) Crystal structure of the P22 TSP (PBD: 1TYX)[97] with the O-antigen substrate bound in the catalytic pocket. The D392 residue is highlighted in pink. (c) Schematic representation of O-antigen digestion by phage P22 hosting an enzymatically active TSP. (d) 12% LPS PAGE profiles showing LPS levels from wild-type *S. enterica* treated with different concentrations of purified TSP (wild-type or D392N mutant) for 10 minutes at room temperature. LPS extracted from the Δ*waaL* strain is shown as a control. (e) Ten-fold serial dilution spot assay of P22 phage on wild-type *S. enterica* treated with 10 nM purified TSP. The image is representative of triplicate experiments. (f, g) Protectiveness of the wild-type *S. enterica* strain treated with purified TSP (wild-type or D392N mutant) relative to the mock-treated *S. enterica* after competition with *E. cloacae* wild-type (f) or Δ*tssM* (g) strains. Data in (f, g) are presented as means ± SD (n=6). Asterisks indicate statistically significant differences between the relative protective index of TSP-treated *S. enterica* and the mock-treated control ($p < 0.05$).

Figure 5

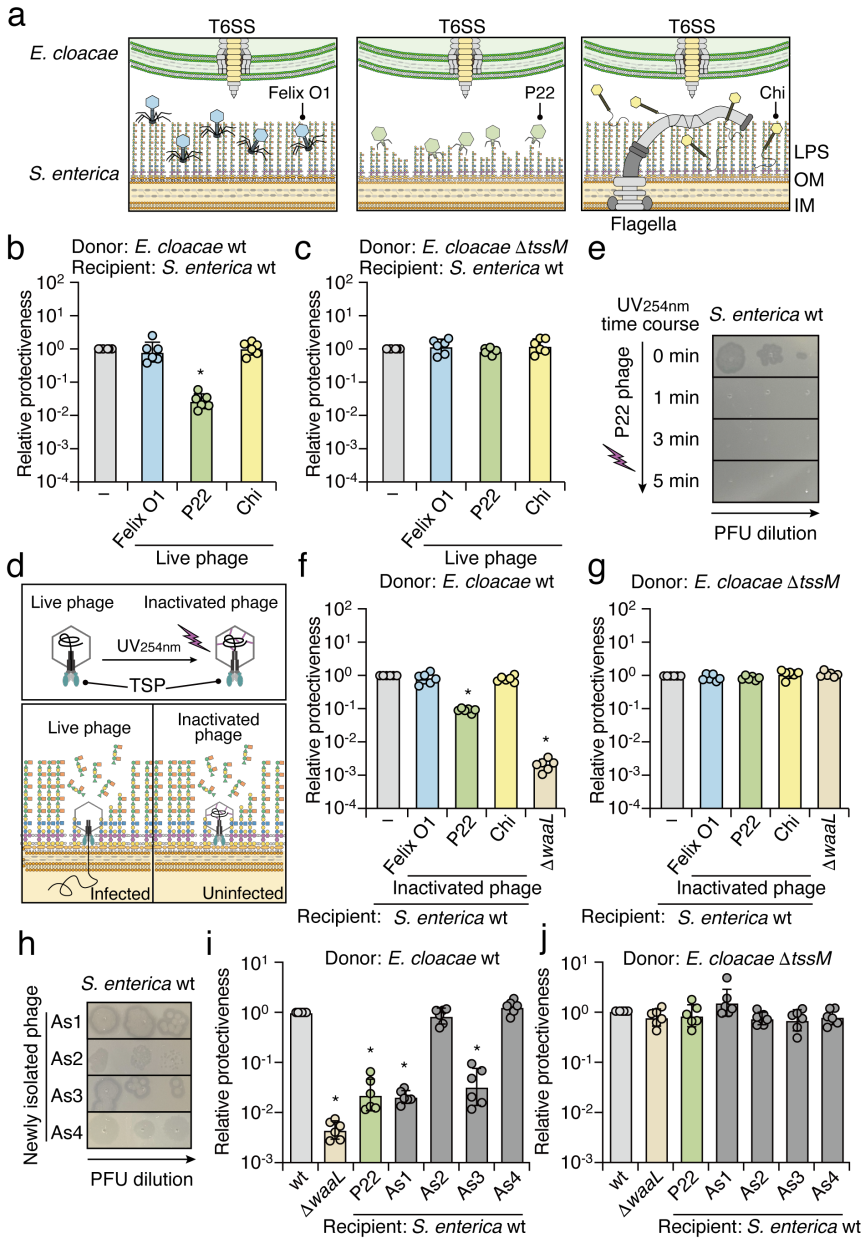

Figure 5. Phage P22 sensitizes *S. enterica* to T6SS-mediated attacks in mixed populations. (a) Schematic representation of phages with or without LPS-targeting endoglycosidase during infection of S. *enterica*. *E. cloacae* carrying a functional T6SS is depicted at the top. (b, c) Protectiveness of the wild-type *S. enterica* strain treated with different phages (Felix O1, P22, or Chi) relative to the mock-treated *S. enterica* after competition with *E. cloacae* wild-type (b) or Δ*tssM* (c) strains. (d) Schematic of P22 with UV_{254nm} treatment. (e) Ten-fold serial dilution spot assay of UV-inactivated P22 phage on wild-type *S. enterica*. The image is representative of triplicate experiments. (f, g) Protectiveness of the wild-type *S. enterica* strain treated with UV-inactivated phage particles (Felix O1, P22, or Chi) relative to the mock-treated *S. enterica* after competition with *E. cloacae* wild-type (f) or Δ*tssM* (g) strains. (h) Ten-fold serial dilution spot assay of phages As1, As2, As3, and As4. (i, j) Protectiveness of the wild-type *S. enterica* strain treated with different phages (P22, As1, As2, As3, or As4) relative to the mock-treated *S. enterica* after competition with *E. cloacae* wild-type (i) or Δ*tssM* (j) strains. Data in (b, c, f, g, i, j) are presented as means ± SD (n=6). Asterisks indicate statistically significant differences between the relative protective index of phage-treated or UV-inactivated phage-treated *S. enterica* and the mock-treated control ($p < 0.05$).

1105 Figure 6

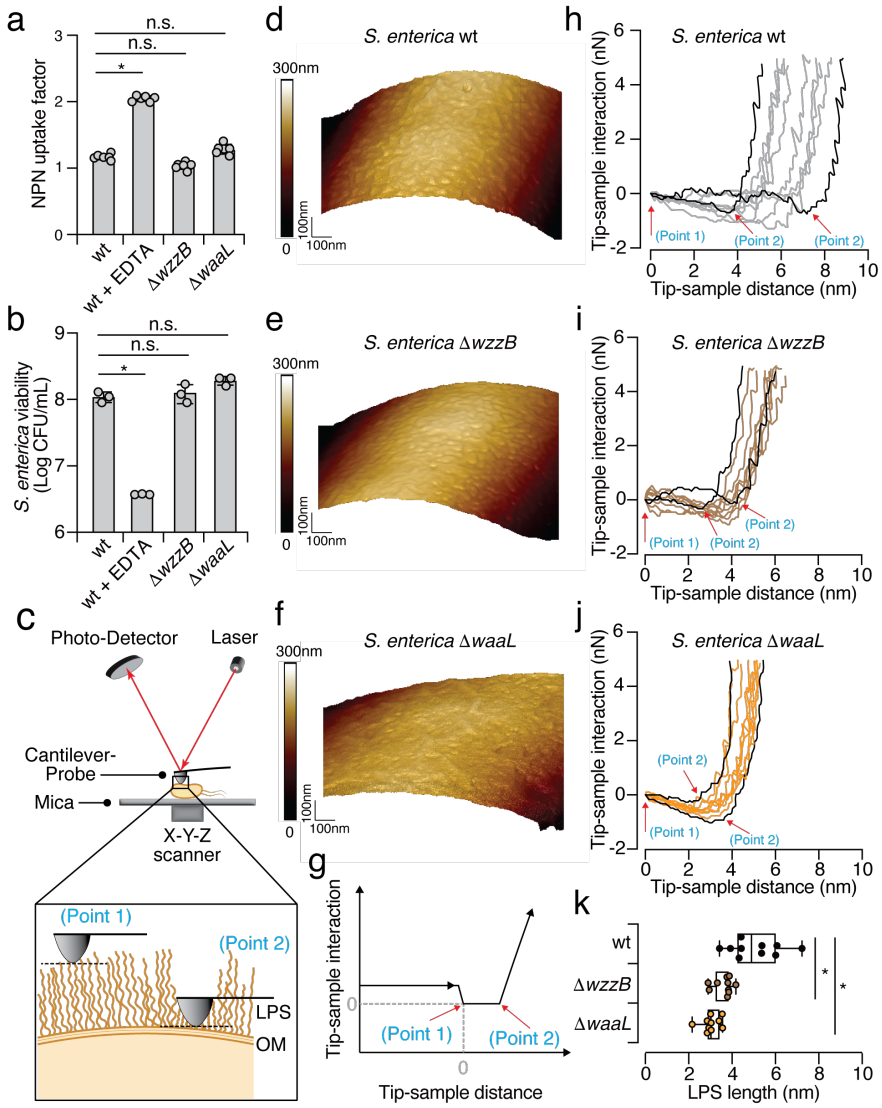

Figure 6. Evidence that the O-antigen of LPS serves as a physical barrier. (a, b) Measurements of outer membrane permeability of the *S. enterica* wild-type, Δ*wzzB*, and Δ*waaL* strains. EDTA (1 mM) was added to the wild-type as the control. (a) NPN uptake assay; (b) VAN sensitivity assay. (c) Schematic representation of the atomic force microscopy (AFM) setup. *S. enterica* cells were immobilized on freshly prepared mica substrates. A laser beam reflected on the back of the cantilever is used to measure the force interactions between the probe and sample. The feedback control system between the photodetector and the X-Y-Z scanner enables precise detection of the surface morphology of the cells. A zoomed-in view of AFM measurement of the bacterial surface is also shown. (d-f) Images of AFM height for the *S. enterica* wild-type (d), Δ*wzzB* (e), and Δ*waaL* (f) strains, as obtained using the PeakForce Tapping (PFT) mode. The image scan size is 1 µm x 1 µm. (g) Schematic of the AFM force-distance curve obtained from *S. enterica* samples using the Force Volume (FV) mapping mode. The point at which the tip contacts the sample is defined as zero (point 1), and slope changes indicate a transition to a stiffer substrate (point 2). (h-j) Force-distance curves for the *S. enterica* wild-type (h), Δ*wzzB* (i), and Δ*waaL* (j) strains. Ten curves were captured from each sample at randomly selected locations, with the longest and shortest LPS lengths highlighted. Red arrows mark points 1 and 2. (k) LPS length of the *S. enterica* wild-type, Δ*wzzB*, and Δ*waaL* strains was determined from force-distance curves by measuring the distance between point 1 and point 2.

1106

Figure 7

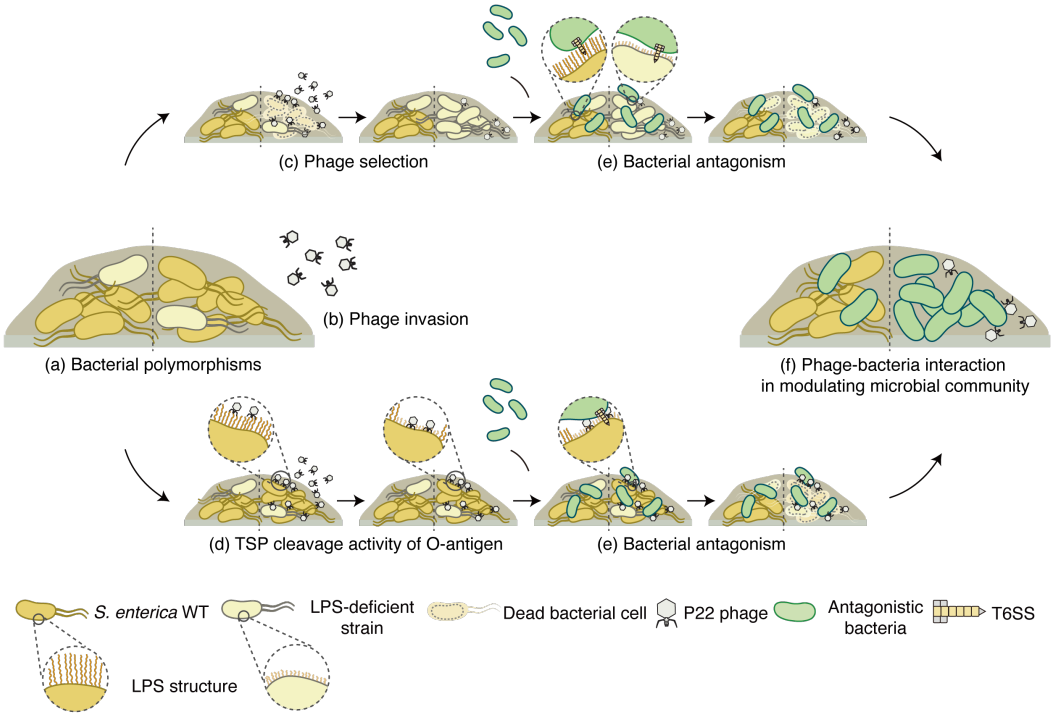

Figure 7. Working model of how phages modulate interbacterial competition within microbial communities. Bacterial interactions are shaped either by the absence (left) or presence (right) of phages. (a) Bacteria inhabit polymorphic environments. (b) In the presence of P22 phage, bacterial surfaces can be modified via two distinct mechanisms. (c) LPS-modified strains are selected due to their resistance to phage adsorption, leading to their dominance within *S. enterica* populations. (d) TSP from P22 phage specifically cleaves the bacterial O-antigen of LPS, resulting in a shortened structure. (e) LPS deficiency increases the susceptibility of *S. enterica* to contact-dependent killing by bacterial competitors in close proximity. (f) Phage-mediated surface modifications influence the outcome of interbacterial competition, driving dynamic shifts in mixed bacterial populations.

Supplementary Figure 1

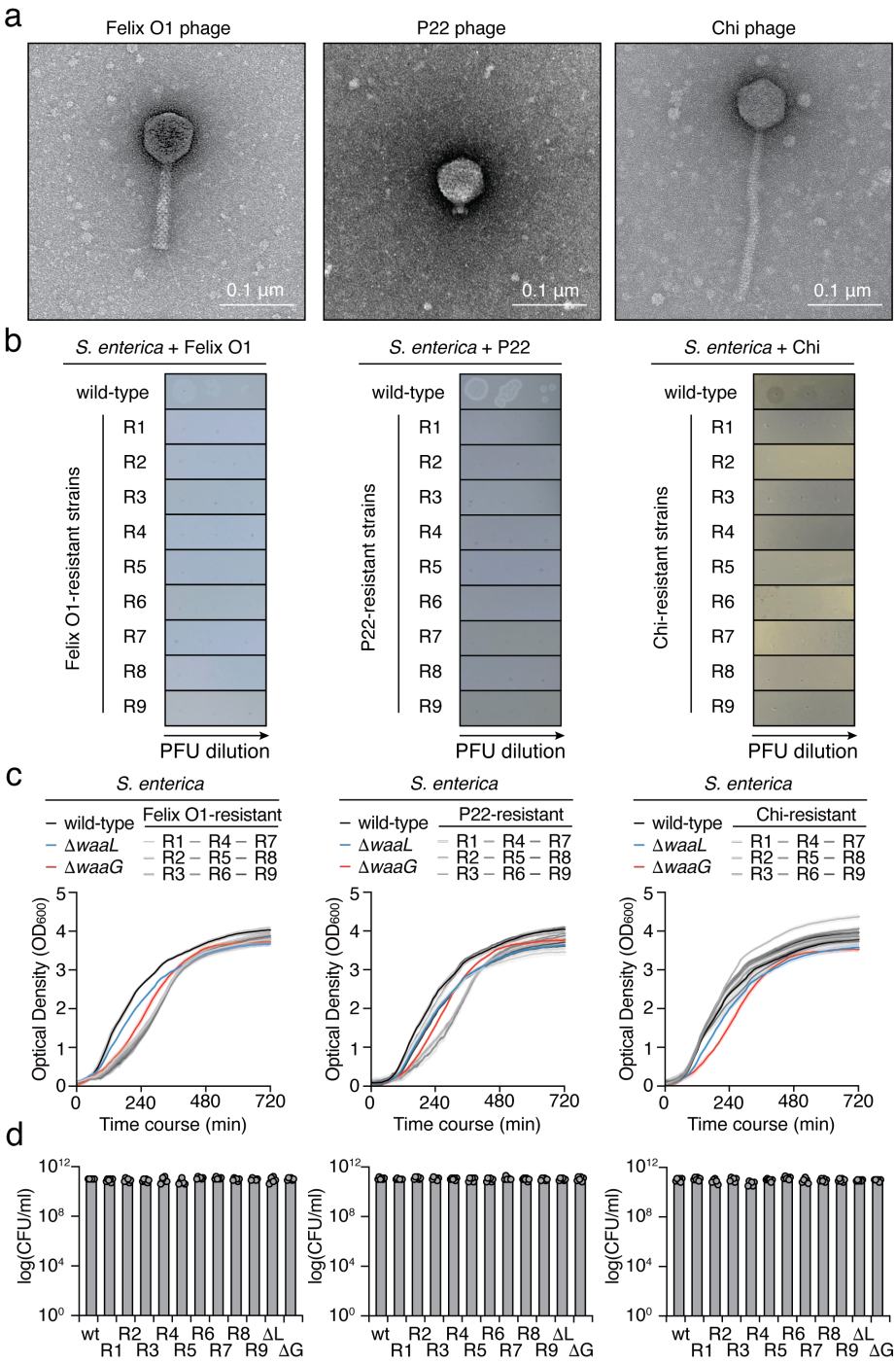

Figure S1. Validation of phage resistance in isolated mutants and monocultural growth experiments. (a) TEM images of model phages used in the study: Felix O1 (left), P22 (middle), and Chi (right). Scale bar = 0.1 µm. (b) Ten-fold serial dilution spot assay of phages Felix O1 (left), P22 (middle), and Chi (right) on the indicated phage-resistant *S. enterica* strains. The image is representative of triplicate experiments. (c) Growth curves of the indicated phage-resistant *S. enterica* strains in LB broth at 37 °C. Wild-type, Δ*waaL*, and Δ*waaG* strains are shown as controls. (d) CFUs of the indicated phage-resistant *S. enterica* strains grown at 37 °C for 12 hours on LB agar plates. Wild-type, Δ*waaL* (ΔL), and Δ*waaG* (ΔG) strains are shown as controls.

Supplementary Figure 2

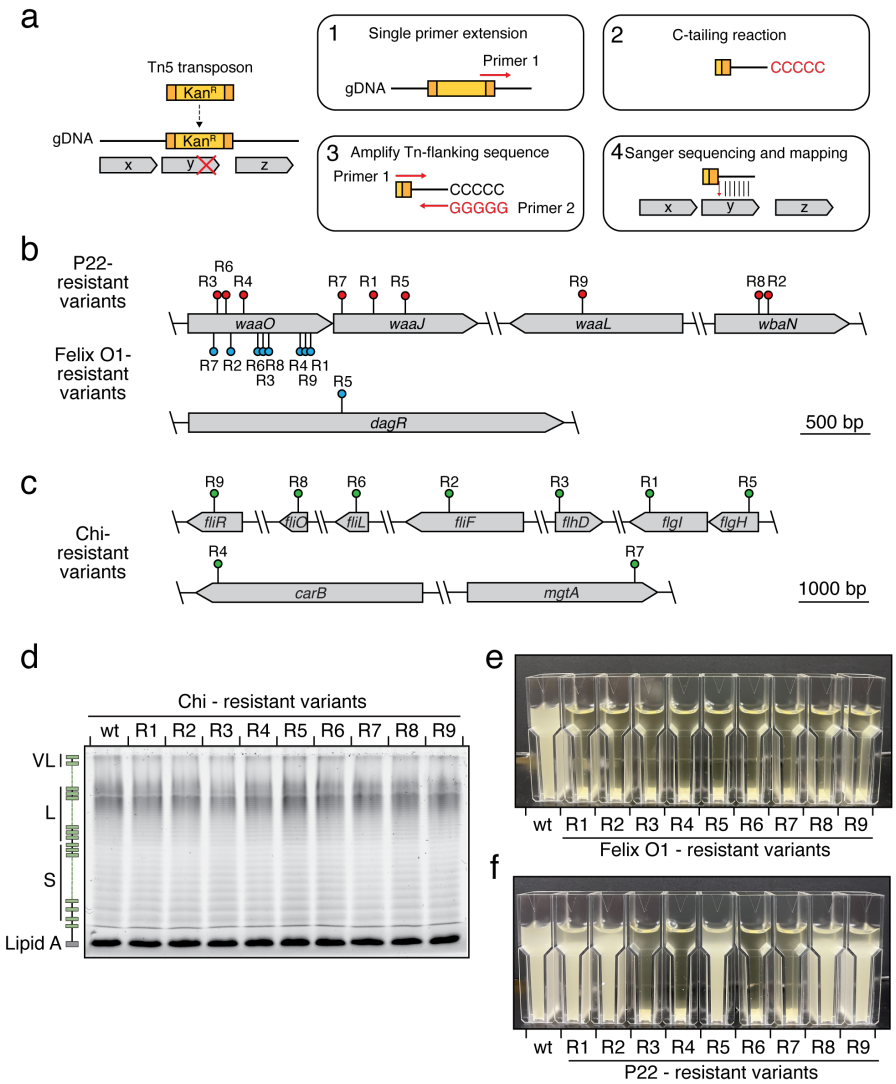

Figure S2. Characterization of transposon insertion mutations in phage-resistant *S. enterica* isolates. (a) Schematic workflow for identifying phage-resistant mutations. Detailed procedures are provided in the Methods section. (b) Mutated genes in the P22-resistant and Felix O1-resistant *S. enterica* isolates. Scale bar = 500 bp. (c) Mutated genes in the Chi-resistant *S. enterica* isolates. Scale bar = 1000 bp. (d) 12% LPS PAGE profiles showing LPS levels from the indicated Chi-resistant *S. enterica* strains. A schematic representation of LPS is shown on the left. (e, f) Macroscopic aggregation analysis to assess LPS deficiency in the indicated Felix O1-resistant (e) or P22-resistant (f) *S. enterica* strains. The images are representative of triplicate experiments.

1108

1109

Supplementary Figure 3

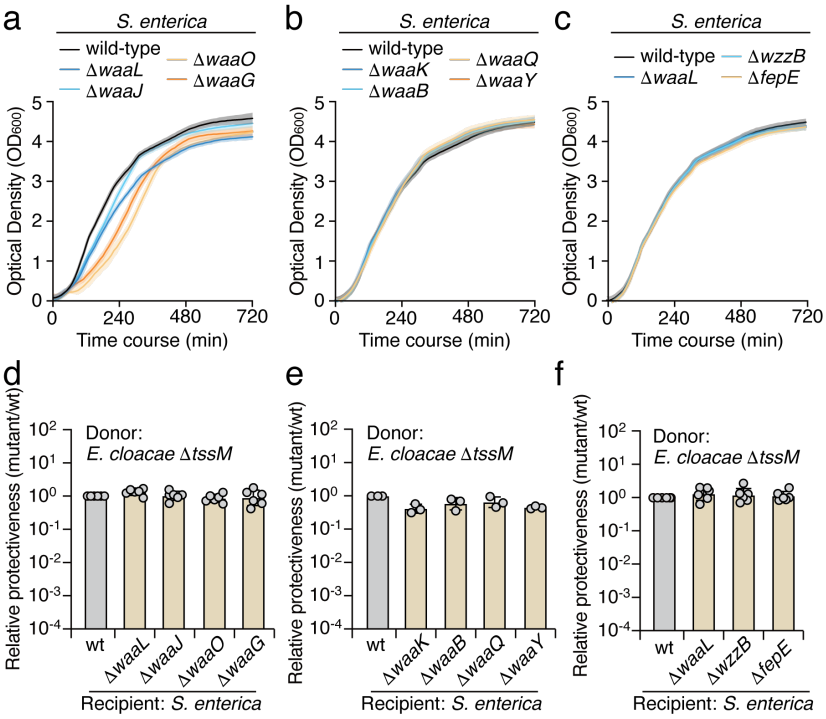

Figure S3. LPS-deficient *S. enterica* mutants exhibit no significant growth or competition defects. (a-c) Growth curves of the indicated *S. enterica* LPS mutants in LB broth at 37 °C. The wild-type strain is shown as a control. (d-f) Protectiveness of the indicated *S. enterica* mutant strains relative to the wild-type strain after competition with *E. cloacae* Δ*tssM*. Data in (d-g) are presented as means ± SD (n=6).

1110

Supplementary Figure 4

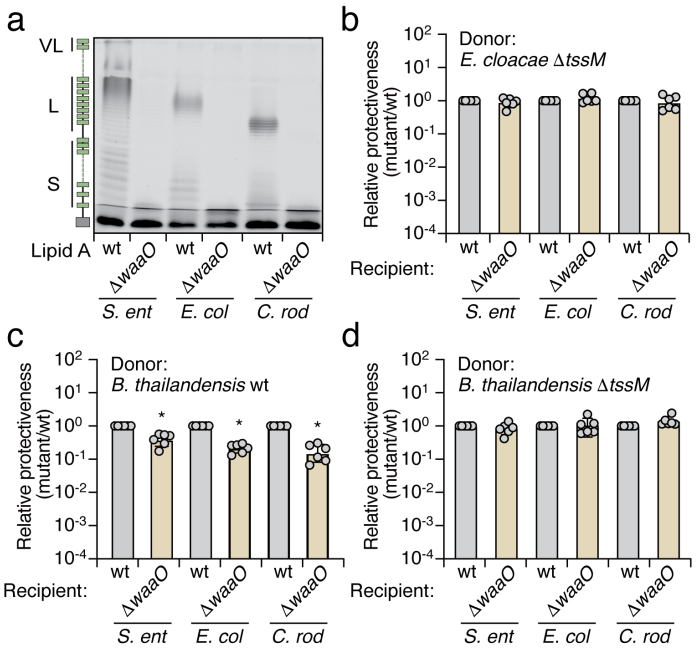

Figure S4. LPS-deficient bacteria exhibit fitness deficits in competition with antagonistic bacteria carrying active T6SS. (a) 12% LPS PAGE profile displaying LPS levels produced by the indicated *S. enterica*, *E. coli*, and *C. rodentium* strains. **(b)** Protectiveness of the indicated bacterial species (Δ*waaO* mutant) relative to the wild-type strain after competition with *E. cloacae* Δ*tssM*. **(c, d)** Protectiveness of the indicated bacterial species (Δ*waaO* mutant) relative to the wild-type strain after competition with *B. thailandensis* wild-type **(c)** or Δ*tssM* **(d)** strains. Data in **(b-d)** are presented as means ± SD (n=6). Asterisks indicate statistically significant differences in the relative protective index between the mutant and wild-type strains ($p < 0.05$).

1111

Supplementary Figure 5

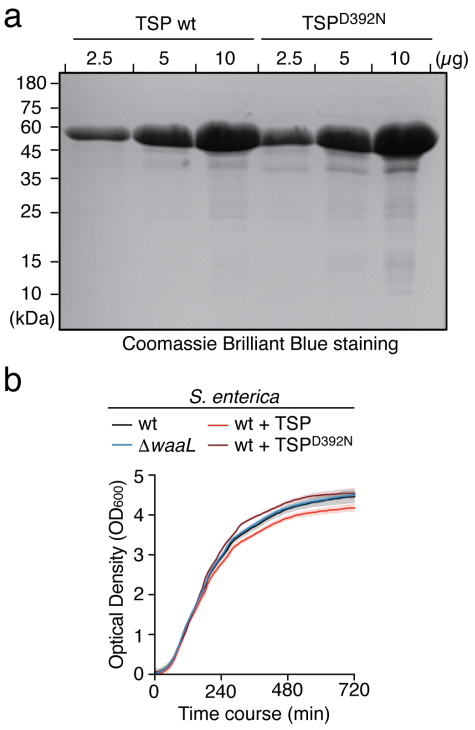

Figure S5. TSP-treated *S. enterica* shows no significant growth defect. (a) Coomassie-stained 12.5% SDS-PAGE analysis of the purified TSP (left) and the D392N catalytic mutant (right). (b) Growth curves of wild-type *S. enterica* incubated with 10 nM of purified TSP (wild-type or D392N mutant) at 37 °C. Mock-treated wild-type *S. enterica* and the Δ*waaL* mutant are shown as controls.

1112

Supplementary Figure 6

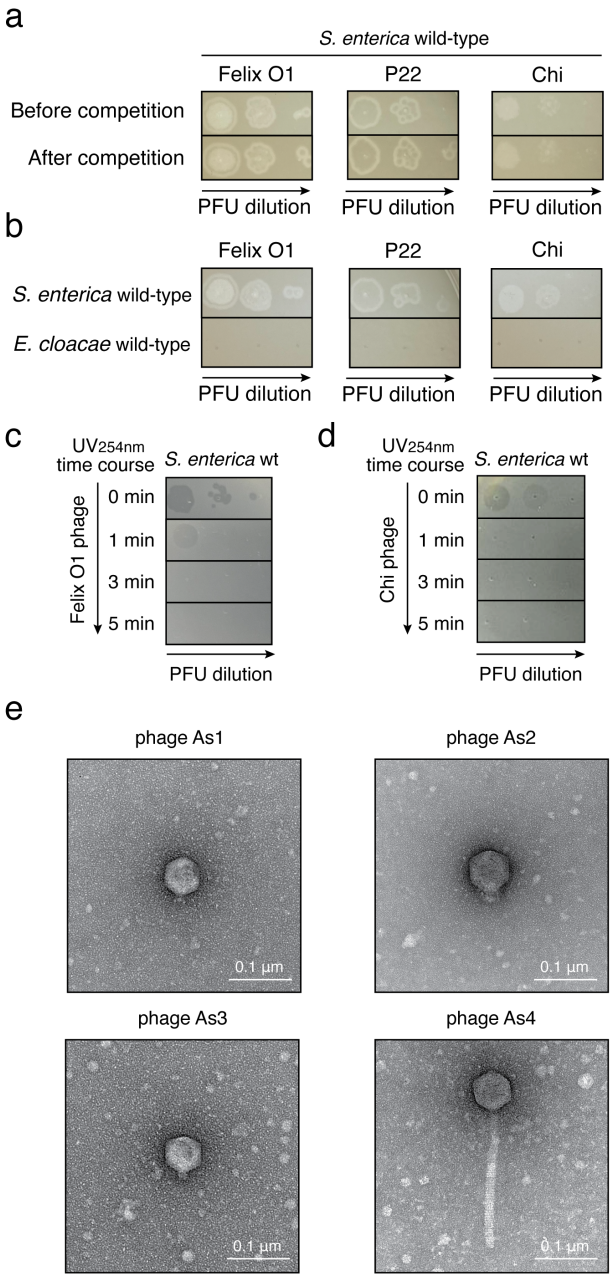

Figure S6. Supporting evidence that phage P22 sensitizes *S. enterica* to T6SS-mediated attacks. (a) Ten-fold serial dilution spot assay of phages Felix O1 (left), P22 (middle), and Chi (right) on wild-type *S. enterica* before and after the competition assay (**Figure 5b**). (b) Ten-fold serial dilution spot assay of phages Felix O1 (left), P22 (middle), and Chi (right) on wild-type *S. enterica* and *E. cloacae*. (c, d) Ten-fold serial dilution spot assay of UV-inactivated Felix O1 phage (c) or Chi phage (d) on wild-type *S. enterica*. The images are representative of triplicate experiments. (e) TEM images of isolated phages used in the study: As1 (top left), As2 (top right), As3 (bottom left), and As4 (bottom right). Scale bar = 0.1 µm.

1113

Supplementary Figure 7

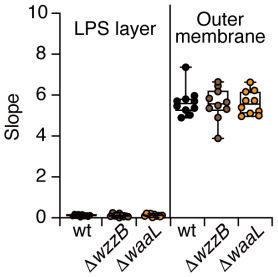

Figure S7. The slope of AFM force-distance curves. Two distinct slopes from each force-distance curve were obtained for the *S. enterica* wild-type, Δ*wzzB*, and Δ*waaL* strains. Ten curves were divided into two segments by point 2, as shown in **Figure 6g**. The slope measured from the first segment corresponds to the LPS layer (left), whereas the second segment represents the outer membrane (right).